ERDC SR-23-1

US Army Corps
of Engineers®
Engineer Research and
Development Center

ERDC
ENGINEER RESEARCH & DEVELOPMENT CENTER

Establishing a Series of Dust Event Case Studies for North Africa

Kent H. Sparrow and Sandra L. LeGrand

February 2023

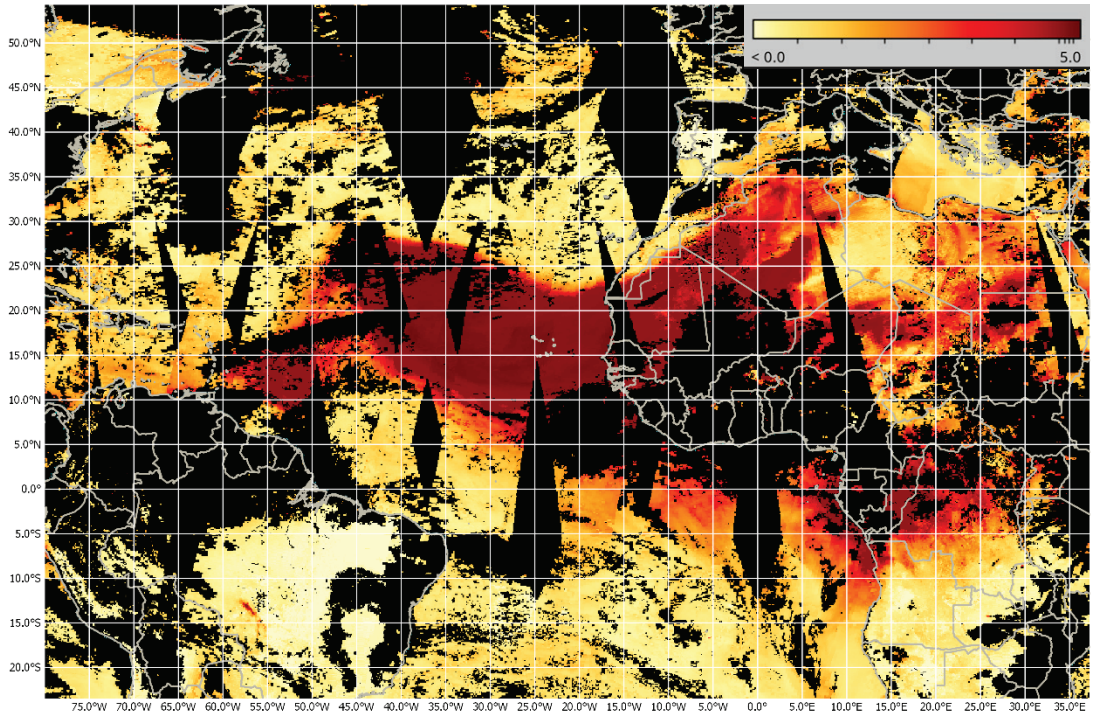

Engineer Research and
Development Center

The US Army Engineer Research and Development Center (ERDC) solves the nation's toughest engineering and environmental challenges. ERDC develops innovative solutions in civil and military engineering, geospatial sciences, water resources, and environmental sciences for the Army, the Department of Defense, civilian agencies, and our nation's public good. Find out more at www.erdc.usace.army.mil.

To search for other technical reports published by ERDC, visit the ERDC online library at https://erdclibrary.on.worldcat.org/discovery.

ERDC SR-23-1
February 2023

Establishing a Series of Dust Event Case Studies for North Africa

Kent H. Sparrow

Coastal and Hydraulics Laboratory
3909 Halls Ferry Road
Vicksburg, MS 39180-6199

Sandra L. LeGrand

Geospatial Research Laboratory
7701 Telegraph Road
Alexandria, VA 22315

Final report

Prepared for Air Force Lifecycle Management Center and
United Kingdom Meteorology Office
Hanscom AFB, MA 01731-2103

Under MIPR F2BDAN1239G003

Abstract

Dust aerosols often create hazardous air quality conditions that affect human health, visibility, agriculture, and communication in various parts of the world. While substantial progress has been made in dust-event simulation and hazard mitigation over the last several decades, accurately forecasting the spatial and temporal variability of dust emissions continues to be a challenge. This report documents an analysis of atmospheric conditions for a series of dust events in North Africa. The researchers highlight four analyzed events that occurred between January 2016 to present in the following locations: (1) the western Sahara Desert; (2) East Algeria and the Iberian Peninsula; (3) Chad-Bodélé Depression; (4) Algeria and Morocco. For each event, the researchers developed an overview of the general synoptic, mesoscale, and local environmental forcing conditions that controlled the event evolution and used a combination of available lidar data, surface weather observations, upper-air soundings, aerosol optical depth, and satellite imagery to characterize the dust conditions. These assessments will support downstream forecast model evaluation and sensitivity testing; however, the researchers also encourage broader use of these assessments as reference case studies for dust transport, air quality modeling, remote sensing, soil erosion, and land management research applications.

Contents

Figures

Preface

This study was conducted for the Air Force Lifecycle Management Center and the United Kingdom Meteorology Office under the Enhanced Dust Emission Characterization for Improved Atmospheric Dust Forecasting project, MIPR F2BDAN1239G003. The technical monitor was Ms. Sandra LeGrand.

The Hydrologic Systems Branch (HSB) of the Flood and Storm Protection Division (FSPD), US Army Engineer Research and Development Center, Coastal and Hydraulics Laboratory (ERDC-CHL), performed the work. At the time of publication of this report, Dr. Hwai-Ping (Pearce) Cheng was chief, HSB; Dr. Cary A. Talbot was chief, FSPD. The deputy director of the ERDC-CHL was Mr. Keith Flowers, and the director was Dr. Ty Wamsley.

The Information Generation and Management Branch of the Geospatial Research Division, ERDC Geospatial Research Laboratory (GRL), also performed this work. At the time of publication of this report, Mr. Michael F. Mailloux was branch chief, and Mr. Jeffrey B. Murphy was division chief. The deputy director of the ERDC-GRL was Ms. Valerie L. Carney, and the director was Mr. David R. Hibner.

COL Christian Patterson was commander of ERDC, and the director was Dr. David W. Pittman.

1 Introduction

1.1 Background

Dust events can impact human health, travel, agriculture, and communication in various parts of the world (Crook 2009; Bartlett 2004; Schweitzer et al. 2018; Rogowski et al. 2021). Therefore, accurately forecasting dust emissions and transport is of critical importance to society. Researchers from the US Army Engineer Research and Development Center and the United Kingdom Meteorology Office (UK Met Office) are addressing the need to accurately forecast dust emissions and transport by creating a series of dust case study events that can be used as a validation test bed for future dust transport and air quality model simulations. Previous studies indicate that weather forecast models tend to struggle with simulating localized dust plumes and extreme dust hazards, primarily due to poorly characterized dust emissions (e.g., LeGrand and Brooks [2008]). Researchers are working to improve forecasts by enhancing dust-source characterization in forecast models. To further support model research and forecast model testing efforts, the researchers performed an in-depth meteorological analysis of four historical dust events. The selected dust storms range from large, synoptic scale to smaller, mesoscale events to help forecasters determine which forcing mechanisms are handled best by various forecast models. Surface observations, satellite imagery, and reanalysis data provided in this report can be used to guide forecasters in numerical simulations of these dust events. It is expected that these analyses will also help forecasters better understand the development of dust storms across North Africa.

1.2 Objective

The goal of this study was to establish four dust storm case studies and identify atmospheric forcing conditions that led to the initiation and transport of dust plumes for each event. The findings documented in this report can be used to support efforts to determine the sensitivity of forecast models to dust emission scheme modifications and help forecasters understand and predict dust storms across North Africa.

1.3 Approach

The study focused on events that occurred between January 2016 to the present at four locations in North Africa, including the following:

1. The western Sahara Desert
2. The Bodélé Depression in Chad
3. Algeria and Morocco
4. East Algeria and the Iberian Peninsula.

For each event, the researchers described the general synoptic*, mesoscale*, and local environmental forcing conditions that governed dust storm evolution by interpreting lidar data, surface weather observations, upper-air soundings, aerosol optical depth (AOD)*, and satellite imagery. (Note: in this report, the asterisk (*) indicates that its associated word is defined in the appendix.)

To support the in-depth analyses, synoptic (i.e., large-scale) analyses of 600, and 850 hPa[1, 2] level geopotential height* reanalysis data were performed. These geopotential height patterns helped identify the synoptic-scale low- and high-pressure circulations that shaped the storm conditions. The wind speed and direction patterns at these levels were also helpful for identifying jet streaks* in the upper, middle, and lower levels of the atmosphere. Because of the region's limited availability of surface weather station data, the researchers also analyzed wind speed and direction reanalysis data at 10 m above ground level to identify areas of enhanced surface winds that initiated dust lofting into the atmosphere. When available, upper-air atmospheric soundings were examined to analyze wind direction and speed at various atmospheric levels near the dust event.

For the dust conditions, ground-based sunphotometer AOD measurements and spatial plots of satellite-retrieved AOD to survey the atmospheric dust loading associated with each event were used. Satellite-

[1] For a full list of the spelled-out forms of the units of measure used in this document, please refer to *US Government Publishing Office Style Manual*, 31st ed. (Washington, DC: US Government Publishing Office 2016), 248-52, https://www.govinfo.gov/content/pkg/GPO-STYLEMANUAL-2016/pdf/GPO-STYLEMANUAL-2016.pdf.

[2] For a full list of the unit conversions used in this document, please refer to *US Government Publishing Office Style Manual*, 31st ed. (Washington, DC: US Government Publishing Office 2016), 345-7, https://www.govinfo.gov/content/pkg/GPO-STYLEMANUAL-2016/pdf/GPO-STYLEMANUAL-2016.pdf.

based lidar retrievals provided information about the vertical distribution of dust in the atmosphere and helped determine the aerosol type detected. Additionally, the researchers acquired dust-enhanced false-color satellite imagery from the UK Met Office to examine the dust-storm event evolution from beginning to end.

After reviewing these resources, a compiled overview was created to describe the environmental forcing and dust conditions associated with the life cycle of each case study event, with particular emphasis on the conditions governing dust emissions.

2 Methodology

The researchers analyzed reanalysis data, satellite retrievals, and surface observations from various remotely sensed and in situ data sets to analyze the forcing conditions of four dust storm events in North Africa. This effort began by collecting an inventory of dust storm events between 1 January 2016 and 1 August 2021 in the area of interest, using previous literature and social media reports of dust storms for guidance. Once a substantial list of options was achieved, the researchers selected four events for further in-depth analysis based on data availability, geographic location, unique storm characteristics, and the degree to which clouds obscured the dust plume sources in the satellite imagery. The following subsections describe the data resources used to support the storm analyses and supplement locally collected station and sounding observations in more detail.

2.1 Spinning Enhanced Visible InfraRed Imager (SEVIRI) dust-enhanced false-color imagery

The researchers used the 1 km resolution enhanced false-color imagery derived from the Spinning Enhanced Visible InfraRed Imager (SEVIRI) onboard the geostationary Meteosat Second Generation (MSG) satellite to highlight areas of dust, convention*, cloud cover, and other meteorological processes (e.g., Banks and Brindley [2013]; Brindley et al. [2012]). Located 5° W at the equator, the SEVIRI sensor is particularly useful for capturing dust imagery for Africa, Europe, and portions of the Middle East. In the false-color dust product, airborne dust appears bright pink or magenta against dark blue, purple, or white landscapes, and thick clouds have a reddish hue (e.g., Sinclair and Jones [2017]).

2.2 Moderate Resolution Imaging Spectroradiometer (MODIS) aerosol optical depth

Aerosol optical depth is a dimensionless number that relates the amount of aerosol distributed over the vertical column of atmosphere relative to an observation location. It measures the signal attenuation caused by aerosol absorption and scattering as radiation travels through the atmosphere. Generally, an AOD value of less than 0.1 indicates *clean* skies (i.e., maximum visibility), and values greater than 3.0 indicate that the aerosol layer is so dense that it obscures the sun. The researchers reviewed the daily AOD product from the Moderate Resolution Imaging Spectroradiometer

(MODIS) instrument on the NASA Terra (MOD04_L2) and Aqua (MYD04_L2) satellites by using the NASA Worldview portal (https://worldview.earthdata.nasa.gov [last access: 30 August 2021]). Specifically, merged Dark-Target/Deep Blue (DT/DB) AOD layer were used in the analyses because of its combined use for retrieving AOD over a mix of oceans, vegetated/dark soiled land, and desert/arid land (Levy et al. 2013). The DT/DB AOD product derives from observations collected with a swath of approximately 2330 km for each pass, with a sensor resolution of 10 km.

2.3 ERA5 reanalysis data

The researchers performed analyses of synoptic and mesoscale environments for each event using the ERA5 Global Reanalysis data set (Hersbach et al. 2020). This data set, produced by the European Centre for Medium-Range Weather Forecasts (ECMWF), contains a detailed record of global atmosphere conditions from 1950 to present. Though the researchers cannot consider these data to be a form of observations, reanalysis data are a physics-based combination of model-derived data and observations that form a complete and consistent global data set. Analysts commonly rely on reanalysis data to gain a general sense of large-scale and some mesoscale system behavior.

The ECMWF produces ERA5 data on hourly timescales with a horizontal grid resolution of 30 km for 37 pressure levels that extend vertically up to a top level of 0.01 hPa. There are also 2D data available for parameters at the surface or critical heights above the surface, such as 2 m temperature, 2 m dewpoint*, 10 m winds, and surface pressure. Several reanalysis fields were acquired for this study, including the following:

1. U (west-east; zonal) and V (south-north; meridional) wind vector components at the 300, 600, 850 hPa pressure levels.
2. U and V wind vector components for 10 m above the land surface.
3. Geopotential heights for 600 at the 850 hPa pressure levels. Geopotential height on a consistent pressure surface is analogous to pressure as a given height. This helps the researchers reference heights as areas of high and low pressure in the atmosphere.

Following commonly used practices, it was assumed that the 300, 600, and 850 hPa pressure levels from the reanalysis data reflect the general

state of the upper-, mid-, and low-level parts of the atmosphere, respectively.

2.4 Cloud-Aerosol lidar and Infrared Pathfinder Satellite Observation (CALIPSO)

The 532 nm total attenuated backscatter and aerosol subtype profile products derived from the Cloud-Aerosol lidar and Infrared Pathfinder Satellite Observation (CALIPSO) Cloud-Aerosol Lidar with Orthogonal Polarization sensor were used to gain a sense of the vertical structure of each storm (Vaughan et al. 2004). CALIPSO provides vertical distributions of cloud and aerosol layer optical properties measured using dual-wavelength (1,064 nm and 532 nm), dual-polarization, backscatter lidar (Winker et al. 2007). This satellite combines the active lidar instrument with passive infrared and visible imagers to sample the vertical extent of aerosols in the atmosphere (Liu et al. 2008; He and Yi 2015). By using both of the 1,064 nm and 532 nm wavelength returns, postprocessing algorithms can diagnose certain aerosol type classifications, including smoke, volcanic ash, clouds, and dust.

2.5 Aerosol Robotic Network (AERONET)

The Aerosol Robotic Network (AERONET) project consists of a global network of ground-based sunphotometers for measuring AOD (Holben 2001). Observations from AERONET contain three data quality levels, including unscreened (Level 1.0), cloud-screened and quality-controlled (Level 1.5), and quality-assured (Level 2). When available, AOD data at all available levels were used for this study.

3 Event Case Studies

3.1 14–20 June 2020 Sahara Desert

3.1.1 Event overview

The first case study the researchers analyzed occurred in northwestern Africa in the Sahara Desert. This event, commonly referred to by researchers and the media as the *Godzilla* dust storm, began on 14 June, with emissions lasting until 20 June and peak dust emission occurring between 16 June and 18 June. The coverage of the affected area expands across much of the North Africa domain and into parts of the Caribbean Islands and the southeastern United States. During this event, dust aerosol AOD conditions reached the highest magnitude ever measured by satellite with an AOD of 3.5 (Pu and Jin 2021; Francis et al. 2022). The synoptic drivers of this storm were primarily associated with a trough* located to the northwest of Africa over the Atlantic Ocean and a strong subtropical* high-pressure system over northwest Africa. These two circulations enhanced the low-level jet over northwest Africa, a feature known as the Africa Easterly Jet (AEJ). The AEJ combined with downdraft winds from mesoscale convection along the Intertropical Convergence Zone (ITCZ)* resulted in continuous dust emissions for 4 days (Figure 1). Previous analyses indicate that strong southeasterly surface winds brought on by the AEJ, along with strong low-level convergence to lift dust, can generate large-scale dust events in North Africa that transport across great distances (Engelstaedter and Washington 2006; Knippertz and Todd 2012).

Figure 1. Environmental conditions associated with or responsible for dust emissions during the 14–20 June 2020 Sahara Desert *Godzilla* dust storm. The blue H surrounded by dashed lines represents the general location of a strong subtropical high-pressure system. The area outlined by the red box represents the general dust source region, and the red arrows represent the African Easterly Jet (AEJ). Convection occurred to the south in the Intertropical Convergence Zone (ITCZ).

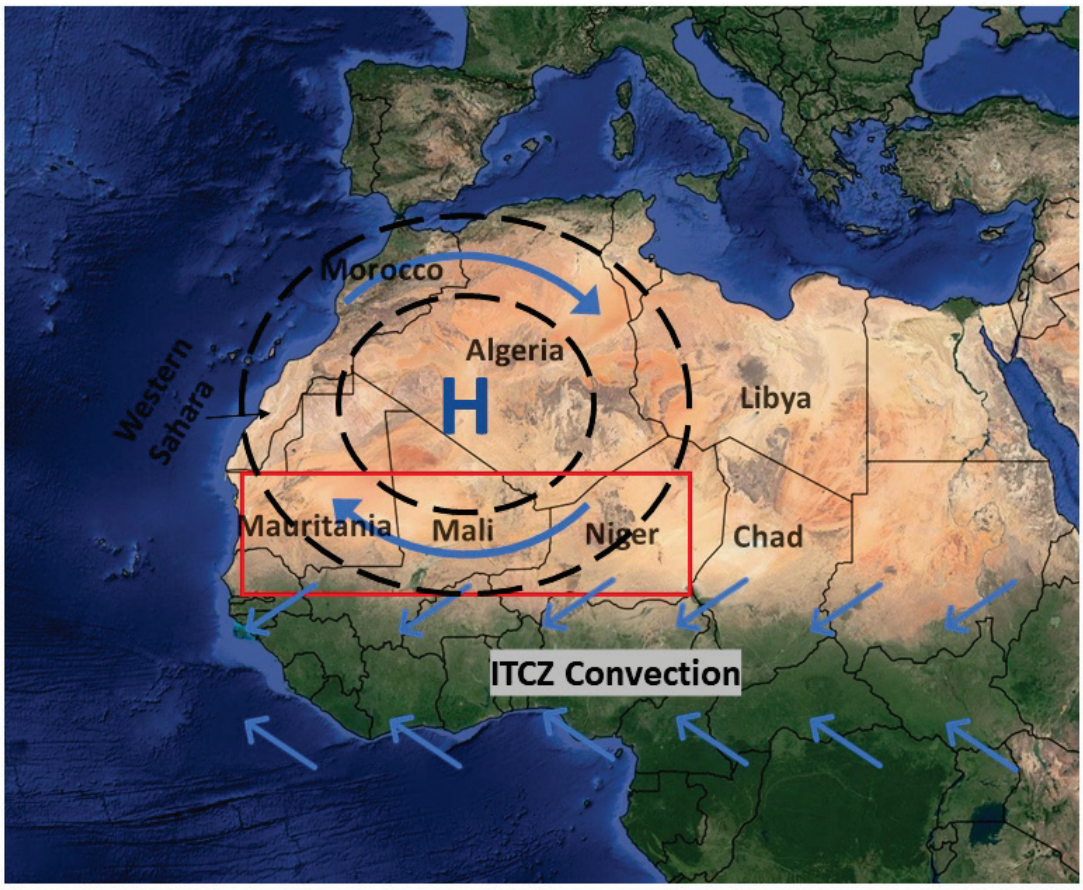

3.1.2 Synoptic overview

The ERA5 600 hPa geopotential height field analysis in Figure 2 displays the synoptic evolution of the event. On 14 June, a large high-pressure ridge* was centered over the border of Algeria and Mali, as indicated by the heights of approximately 4.5 km. A cut-off low is also located to the northwest over the Atlantic Ocean and relatively lower geopotential heights present to the south over the Gulf of Guinea. Between 14 June and 16 June, the ridge drifted westward and moved partially over the Atlantic Ocean and western African coastline. Midlevel winds during this time frame were >30 ms^{-1} along the western and southern portions of the high-pressure circulation due to the tight pressure gradient between the high-pressure circulation and the low-pressure trough to the northwest. The

850 hPa ERA5 wind speed analysis in Figure 3 displays the enhancement of the AEJ throughout the event, as indicated by the strong 850 hPa >20 ms^{-1} wind speeds extending from Niger to Mauritania between 14 June and 16 June. The strong low-level winds mixed down to the surface during this period, as indicated by the strong 10 m surface wind speeds in Figure 4. The strongest 10 m wind speeds extended from the Niger/Algeria border to the coastline of Mauritania, with wind speeds >10 ms^{-1} in some locations. By 17 June, the high-pressure circulation extended well into the Atlantic Ocean, resulting in a strong easterly flow across the western Sahara and parts of the Atlantic. This pattern favored extended dust transport across the Atlantic for the remainder of the event. On 18 June, the high-pressure circulation opened up on its westward side and extended further across the Atlantic towards the Caribbean. By 19 June, the ridge fully merged with the cutoff low, and the midlevel winds subsided across northwestern Africa with strong midlevel winds persisting across the Atlantic.

Figure 2. ERA5 reanalysis of 600 hPa wind speed (ms^{-1}; shaded), geopotential height (m; contoured), and wind barbs valid at 1200 UTC 14–19 June 2020. Strong midlevel winds occur along the southern and western side of the high-pressure circulation.

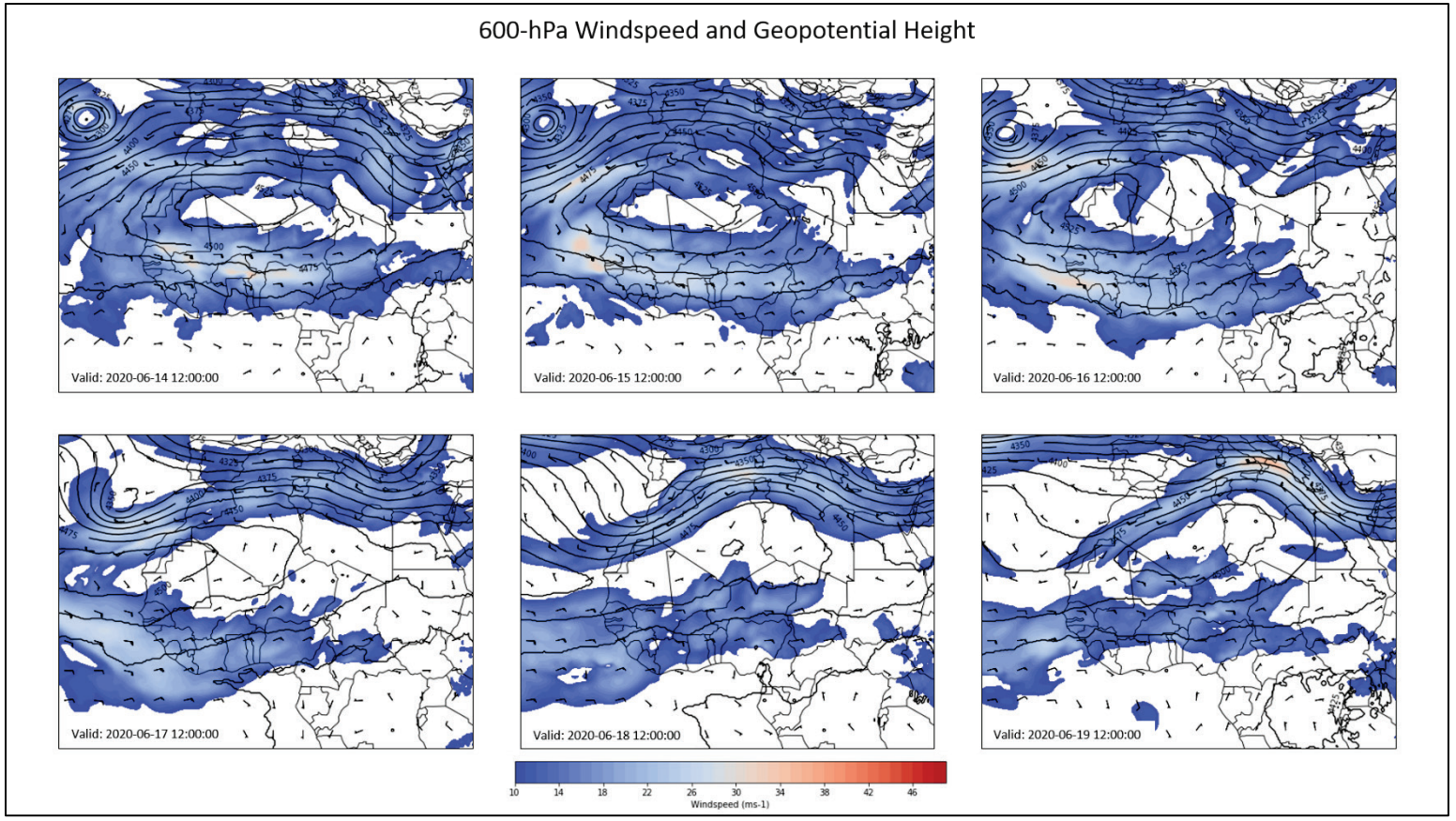

Figure 3. ERA5 reanalysis of 850 hPa wind speed (ms^{-1}; shaded) and wind barbs valid at 1200 UTC 14–19 June 2020. Strong low-level winds from the enhanced African Easterly Jet can be seen across portions of northwestern Africa.

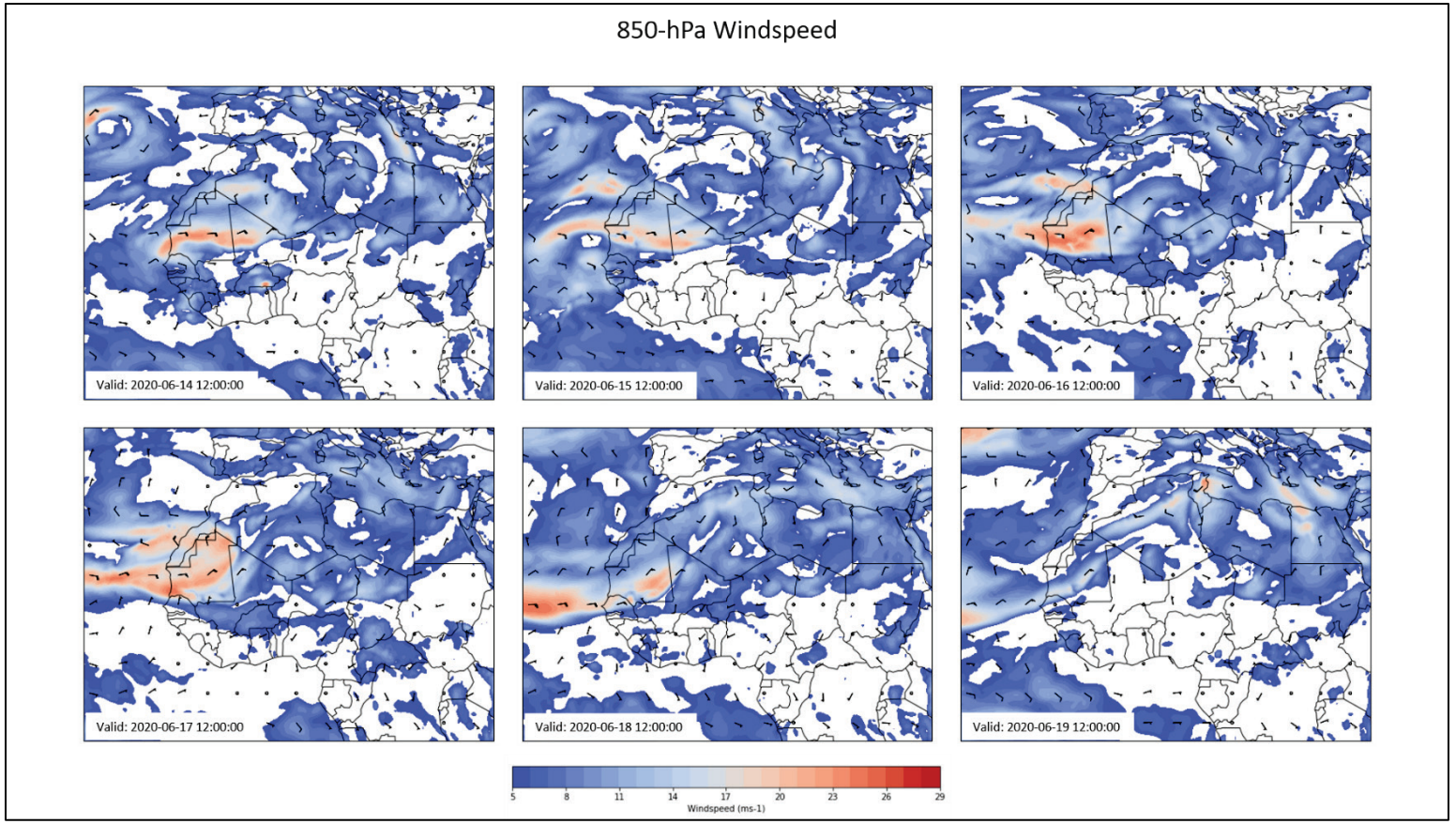

Figure 4. ERA5 Reanalysis of 10 m wind speed (ms^{-1}; shaded) and wind barbs valid at 1200 UTC 14–19 June 2020. Strong surface winds occur across portions of northwest Africa.

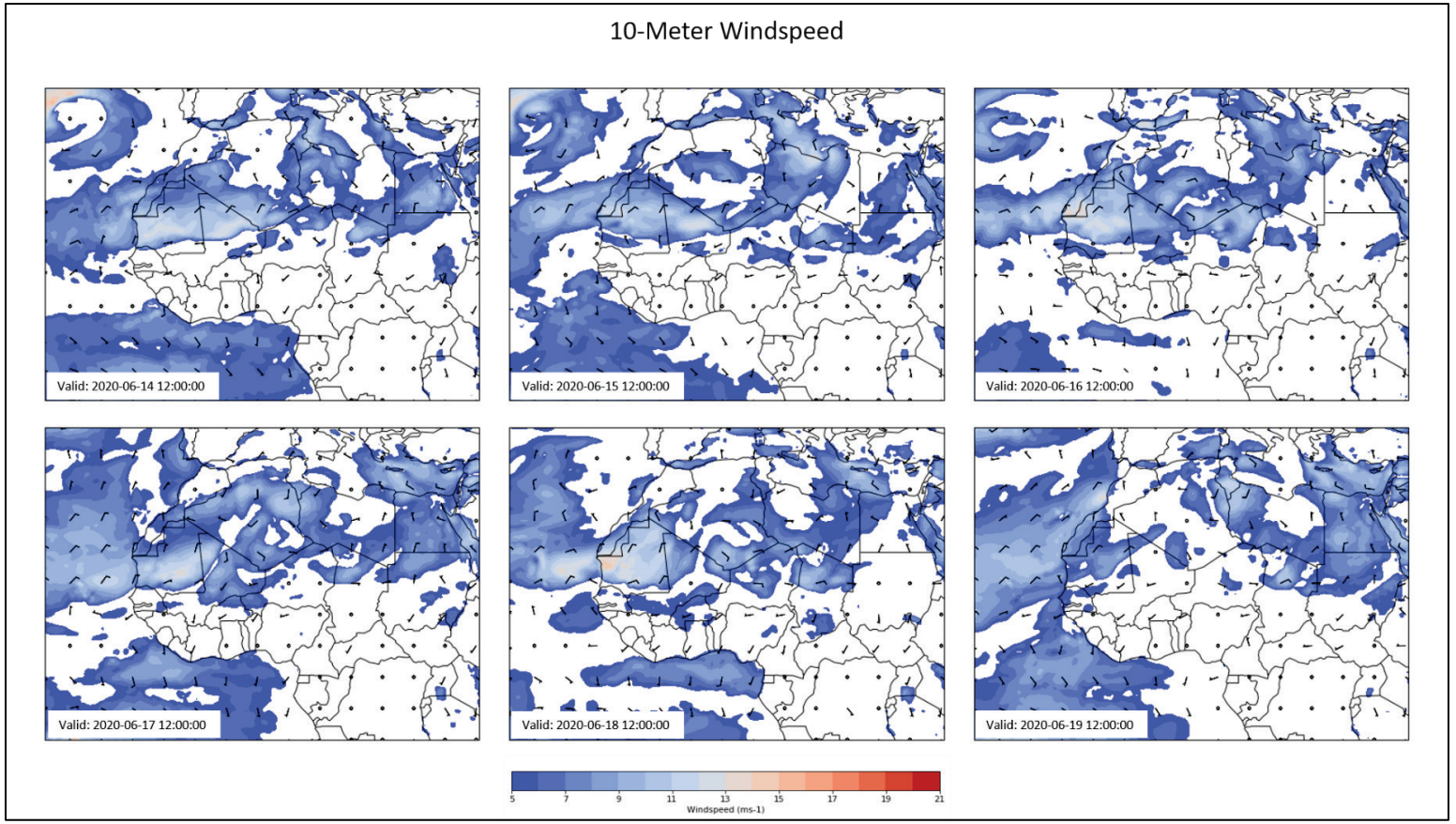

3.1.3 Dust storm evolution

The researchers qualitatively tracked the evolution of the dust storm, which began on 14 June and continued until 20 June, by looking at the dark pink shading of the MSG-SEVIRI imagery. The initiation of the main event on 14 June occurred just north of a mesoscale convective system (MCS)* associated with the ITCZ line of convection extending across central Africa and the Atlantic Ocean. Strong downdrafts associated with the deep convection resulted in a substantial amount of dust lifting into the air on the northern fringes of the MCS. MSG-SEVIRI imagery at 1200 UTC on 14 June displays a large haboob* centered over portions of Chad and Niger with dense cloud cover to the south. Another MCS that occurred along the coastline of Guinea also generated a smaller dust plume over Mauritania. The two plumes were relatively concentrated on 14 June, but the dust propagated westward through the following days while also spreading outward and condensing throughout the region. By1200 UTC on 15 June, an extended dusty area from western Niger to the eastern Atlantic is evident. As dust lofted into the atmosphere, it quickly advected westward once it reached the AEJ area.

Figure 5 also highlights the influence of the strong low-level AEJ winds mixing down to the surface, which resulted in additional dust emissions through 19 June. In addition to the AEJ and mesoscale-driven dust plumes, there may also have been some atmospheric dust loading from the western Africa region known as the intertropical discontinuity zone. This region along the western coast is an area where hot air from the Sahara Desert flows southward to meet air flowing northward from the Gulf of Guinea (Francis et al. 2022; Pospichal et al. 2010). The convergence of wind in this area also possibly contributed to dust being lifted several kilometers into the atmosphere.

Figure 5. MSG-SEVIRI dust-enhanced imagery for 1200 UTC 13–20 June 2020 with arrows pointed at dust plume. Concentrated areas of pink and magenta colors generally indicate airborne dust, while areas of red or brown shading are generally thick clouds.

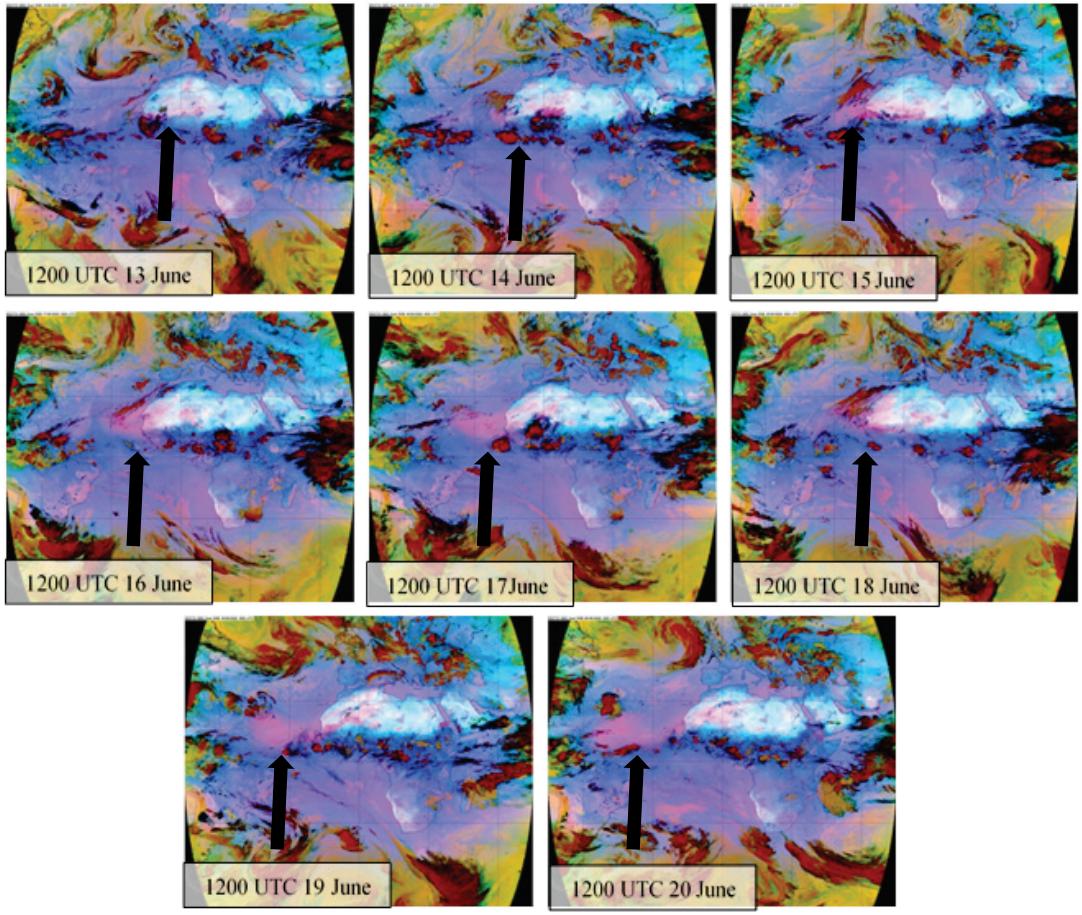

On 16 June, the 0213–0227 UTC CALIPSO 532 nm total attenuated backscatter and aerosol subtype products provided a clear depiction of the vertical distribution of the dust plume (Figure 6). The large area of dust extended up to 5 km into the atmosphere between 0°N–30°N and 0°W–5°W. On 17 June, another large MCS was apparent over Mali, further contributing to the continuous dust emissions. By 18 June, convection associated with the ITCZ began to lull near the dust source region, and strong easterly winds were sweeping the dust plume far out into the Atlantic Ocean. CALIPSO products at 0329 UTC on 18 June (Figure 7) display dust reaching 7 km into the atmosphere between 5°N–25°N and 20°W–24°W.

Figure 6. CALIPSO vertical profile products for 16 June 2020, 0213–0227 UTC. The panel on the top shows the CALIPSO satellite orbit track (pink line) associated with the transect. The 532 nm total attenuated backscatter (km-1 sr-1) product is in the middle, and the aerosol subtype product is on the bottom. The subtypes may include marine aerosol (dark blue), dust (yellow), polluted continental aerosol or smoke (orange), clean continental aerosol (green), polluted dust (brown), elevated smoke (black), dusty marine aerosol (light blue), polar stratospheric clouds (white), volcanic ash (medium grey), or sulfates and other aerosols (dark grey).

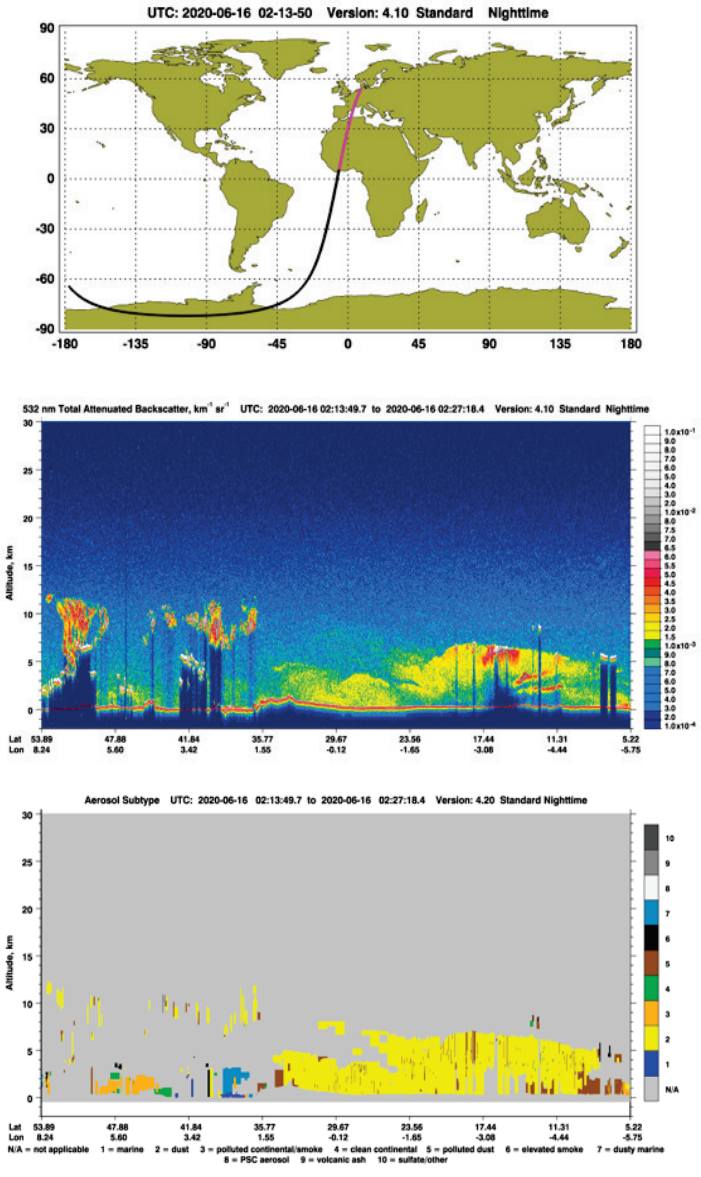

Figure 7. CALIPSO vertical profile products. Same as Figure 6 but for 18 June 2020, 0329–0343 UTC.

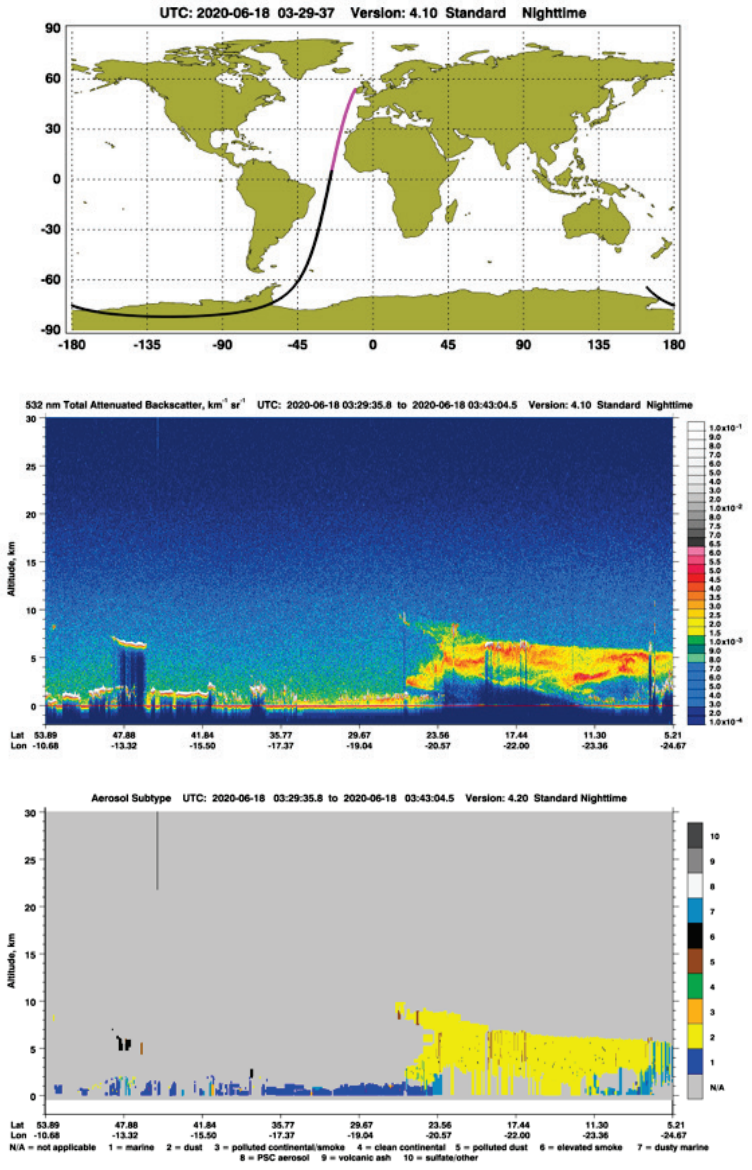

The AOD observations at the AERONET station site on Cape Verde at 16°N and 22.9°W show a peak between 17 June and 19 June as dust transported off the western Sahara and Morocco coastlines. Figure 8 displays the unscreened (level [1] and cloud screened level [1.5]) AOD data. Cloud-screened AOD reached values between 3 and 4 on the 500 nm AOD channel as the dust plume passed directly over the station location. Weather station data observed at Costa Clama (28.16°N, 14.23°W) indicated strong northerly winds with gusts up to 30 mph on 18 June (not pictured). MODIS AOD measurements in Figure 9 show the large dust plume advecting off the west coast of Africa on 18 June. By 19–20 June,

dust emissions subsided across the Sahara, and the massive dust plume tracked toward the Caribbean Sea and the southeastern United States.

Figure 8. Aerosol optical depth at Cape Verde for June 2020, including the level 1 unscreened (left) and level 1.5 cloud-screened (right) data sets. A peak of AOD measurements occur at this AERONET station location approximately 17 June.

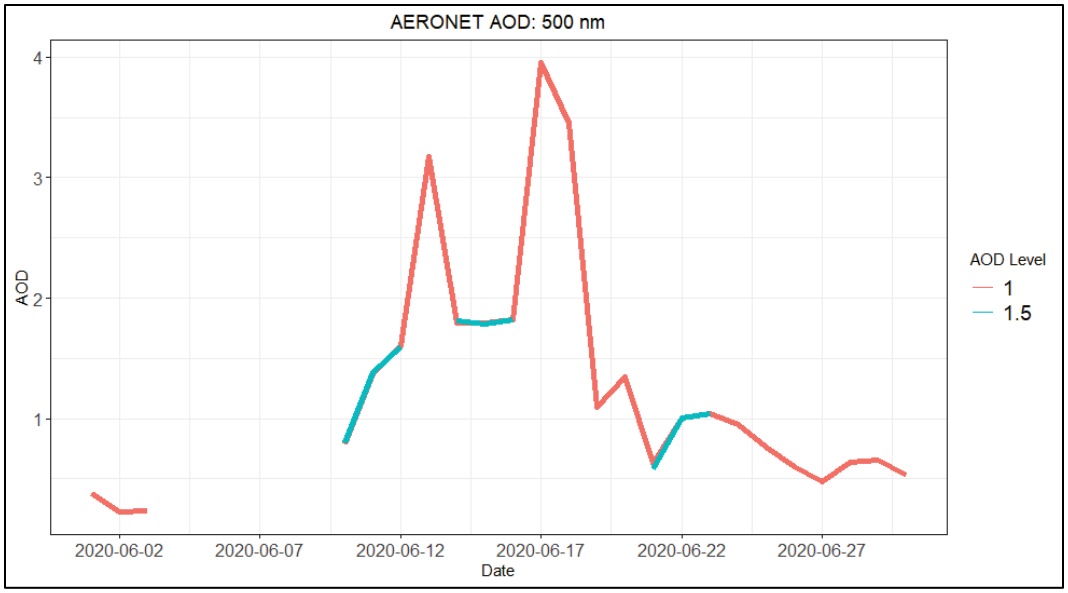

Figure 9. MODIS AOD for 18 June 2020. Note the large dust plume (circled) being transported off the northwest coastline of Africa into the Atlantic.

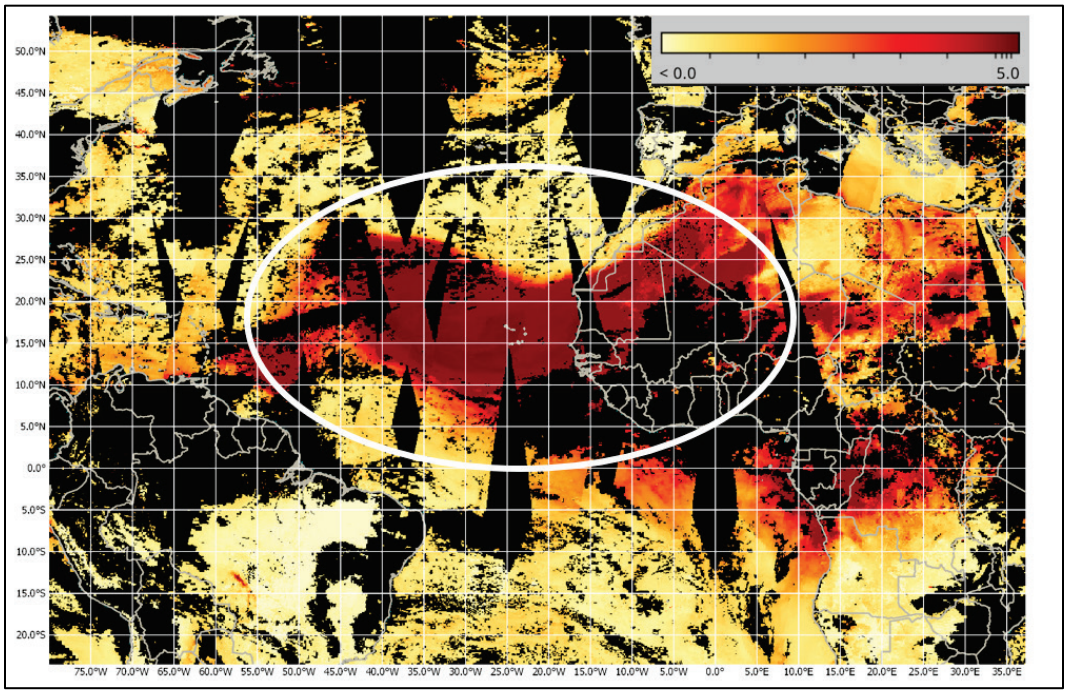

3.2 20 January 2021–Bodélé Depression in Chad

3.2.1 Event overview

The second case study analyzed occurred across the Bodélé Depression in Chad and extended into eastern Niger. The event primarily occurred on 20 January, with most dust emissions beginning around 0800 UTC and continuing through 1800 UTC. Dust emissions were brought on by the funneling of strong low-level winds (approximately 20 ms^{-1}) between the Tibesti and Ennedi mountains when anticyclonic flow around a low-level high-pressure circulation enhanced the Bodélé low-level jet (Figure 10). The wind-funneling effect that occurs between the two mountain ranges with this type of environmental setup frequently brings strong surface winds across the erodible sediments of the Bodélé Depression, making this feature the most prolific source of dust on the planet (Washington et al. 2006, 2009; Prospero et al. 2002). Once lofted, transported dust extended across the Bodélé Depression, over northern portions of Lake Chad, and into the Diffa Region of Niger.

Figure 10. Environmental conditions associated with or responsible for dust emissions during the 20 January 2021 dust storm from the Bodélé Depression in Chad. The blue H surrounded by dashed lines represents the general location of a strong high-pressure system. The area outlined by the black box represents the general dust source region, and the red arrow represents the Bodélé lowel-level jet. The area circled in green depicts the general location of the Bodélé Depression and the area circled in blue is the approximate location of Lak Chad and the Diffa Region of Niger. Convergence of winds through the Mount Tibesti and Mount Ennedi gap create the dust lofting conditions.

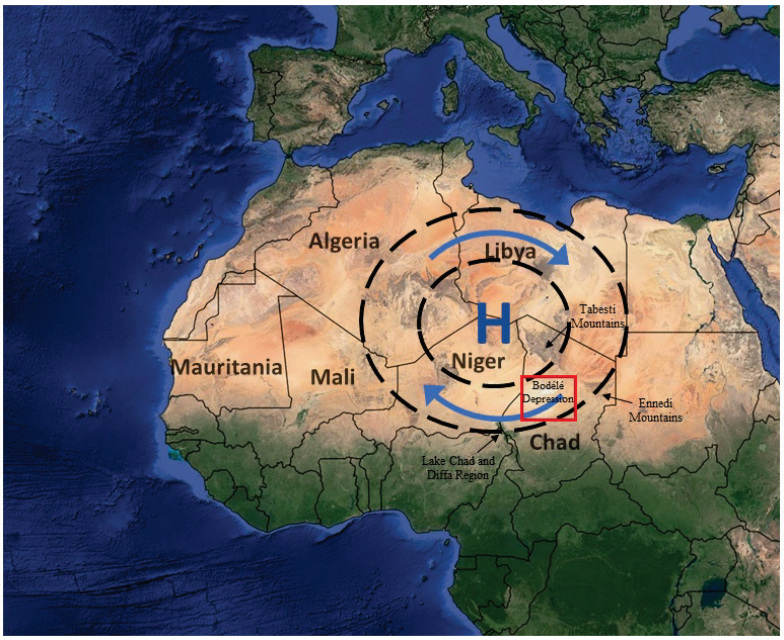

3.2.2 Synoptic overview

Figure 11 shows the ERA5 reanalysis of the 600 hPa synoptic setup for this event. On the 1200 UTC 19 January analysis, a wave train* with a meandering jet-stream pattern extended from the Atlantic, across the Mediterranean Sea, and into the Middle East. A midlevel trough extended across the Mediterranean Sea into Algeria and Libya with a northeasterly flow on the back side of the trough across portions of northern Algeria. On the 1200 UTC 20 January analysis, the pattern shifted eastward, with the trough extending into Egypt and Saudi Arabia. The higher heights that moved in behind the trough were indicative of anticyclonic flow and relatively higher pressure. Higher geopotential heights persisted over the dust source region with little midlevel wind speed or direction change through the 19–20 January period.

The ERA5 reanalysis of 600-hPa winds in shows the evolution of the trough's midlevel winds, which propagated eastward from Algeria and Libya to Egypt and Saudi Arabia between 19–20 January. There is also an apparent high-pressure ridge propagating eastward behind the trough. Relatively calm 600-hPa winds persisted through the 19 January and 20 January 1200 UTC analyses over the dust source region.

Figure 12 displays the ERA5 reanalysis of 850 hPa wind speeds. Midlevel subsidence associated with the ridge on the back side of the trough resulted in an anticyclonic 850 hPa flow, centered over Algeria and Libya. The 1200 UTC 19 January analysis suggests the 850 hPa winds reached speeds of approximately 14 ms^{-1} across portions of Niger and Chad along the eastern side of the ridge. By the 1200 UTC 20 January analysis, northeasterly 850 hPa winds intensified to speeds of approximately 20 ms^{-1}. This enhanced low-level jet setup that extended across Niger and Chad funneled strong winds through the Bodélé Depression, generating the dust event.

The 10 m wind speed analysis shows an enhanced area of surface winds near the border of Niger and Chad in Figure 13. The 1200 UTC 19 January analysis shows winds funneled between the Tibesti and Enedi mountains, reaching speeds of 13 ms^{-1}. By the 1200 UTC 20 January analysis, the winds funneling through this region increased to speeds approximately 17 ms^{-1}.

Figure 11. ERA5 reanalysis of 600 hPa wind speed (ms^{-1}; shaded), geopotential height (m; contoured), and wind barbs valid at 1200 UTC 19–20 January 2021. Note the midlevel wind pattern across North Africa.

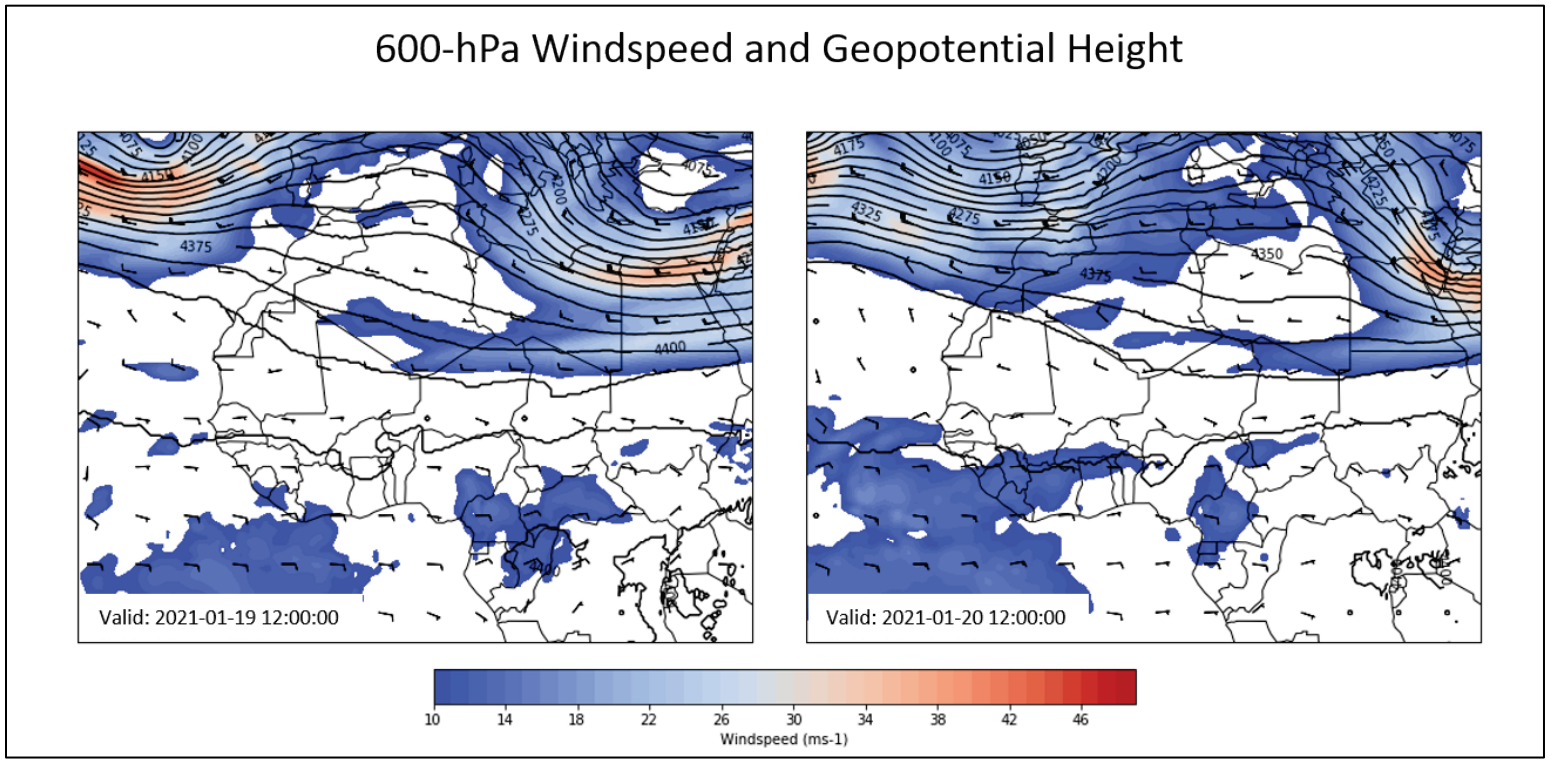

Figure 12. ERA5 reanalysis of 850-hPa wind speed (ms^{-1}; shaded) and wind barbs valid at 1200 UTC 19–20 January 2021. Strong low-level winds form over the Bodélé Depression.

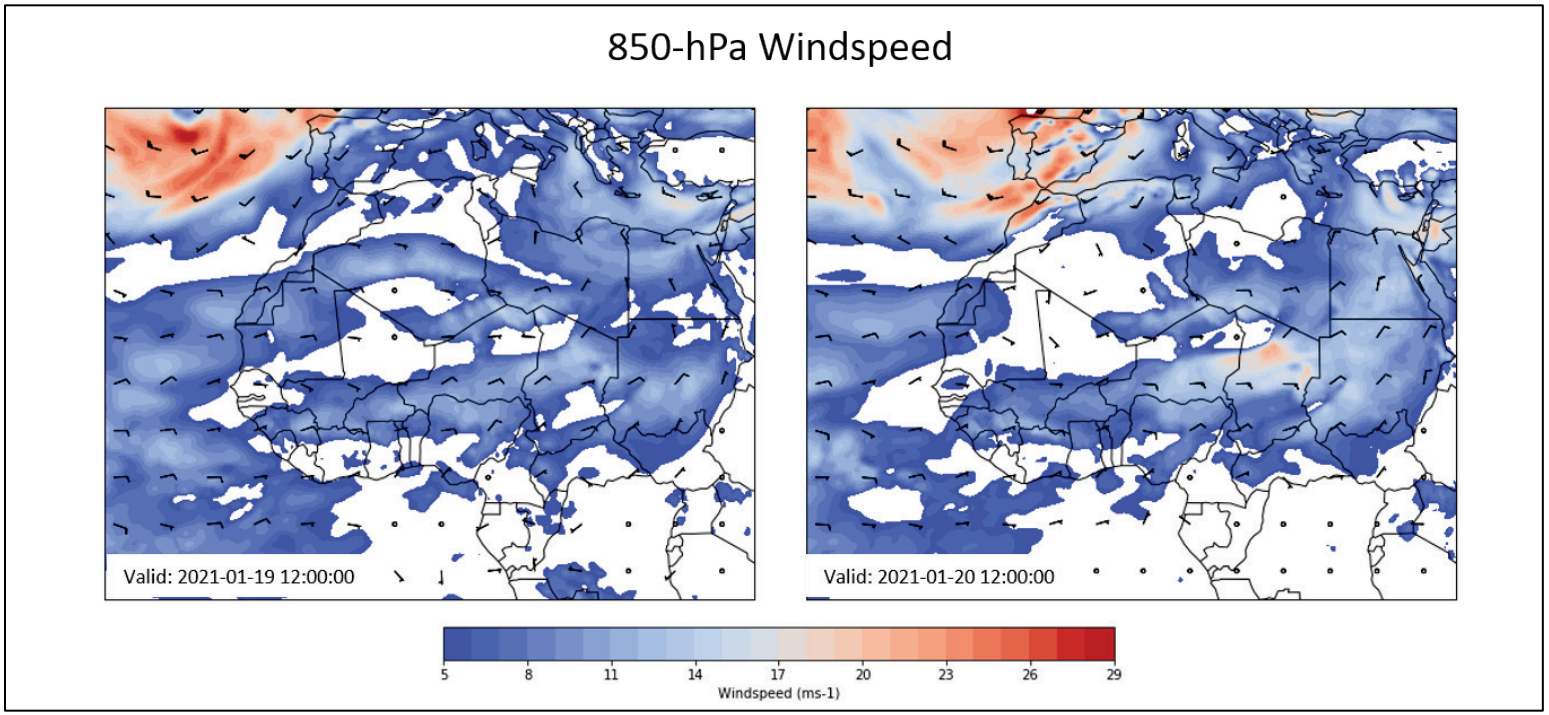

Figure 13. ERA5 Reanalysis of 10 m wind speed (ms^{-1}; shaded) and wind barbs valid at 1200 UTC 19–20 January 2021. Strong surface winds form over the Bodélé Depression.

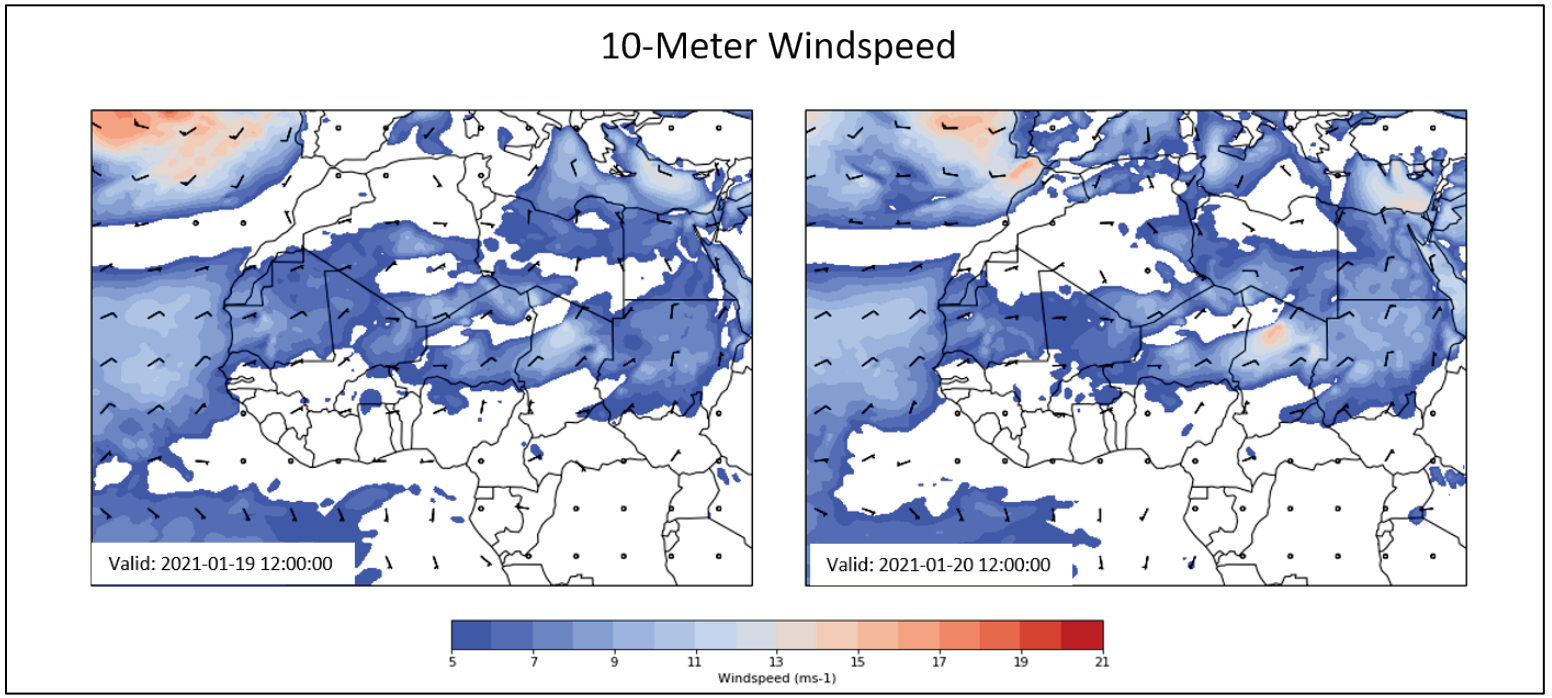

The low-level jet can also be seen near the surface of the 1200 UTC 21 January sounding in Agadez, Niger at 16.96°N and 7.96 °E (Figure 14). East winds at 25–30 knots were observed between the 850 hPa level and the surface.

Figure 14. 1200 UTC 21 January 2021 upper-air sounding for Agadez, Chad.

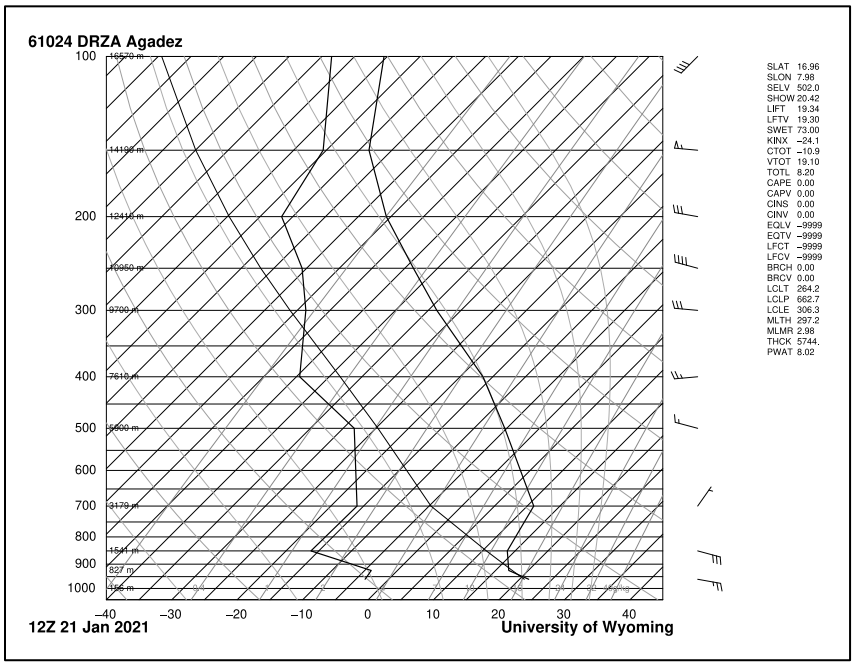

3.2.3 Dust storm evolution

Figure 15 shows the MSG-SEVIRI imagery associated with the dust storm from 0600 to 2200 UTC on 20 January in 2 hr time-steps. The initiation of the event began approximately 1000 UTC as strong winds from the Bodélé low-level jet contacted the surface and rapidly transported a dust plume southwestward. Dust emissions appear to end between 1800 and 2000 UTC. Once the primary dust production mechanism ceased, the dust plume advected southwestward over portions of southern Niger and northern Nigeria.

Figure 15. MSG-SEVIRI dust-enhanced imagery for 0600–2200 UTC 20 January 2021 with arrows pointed at dust plume. Concentrated areas of pink and magenta colors generally indicate airborne dust, while areas of red or brown shading are generally thick clouds.

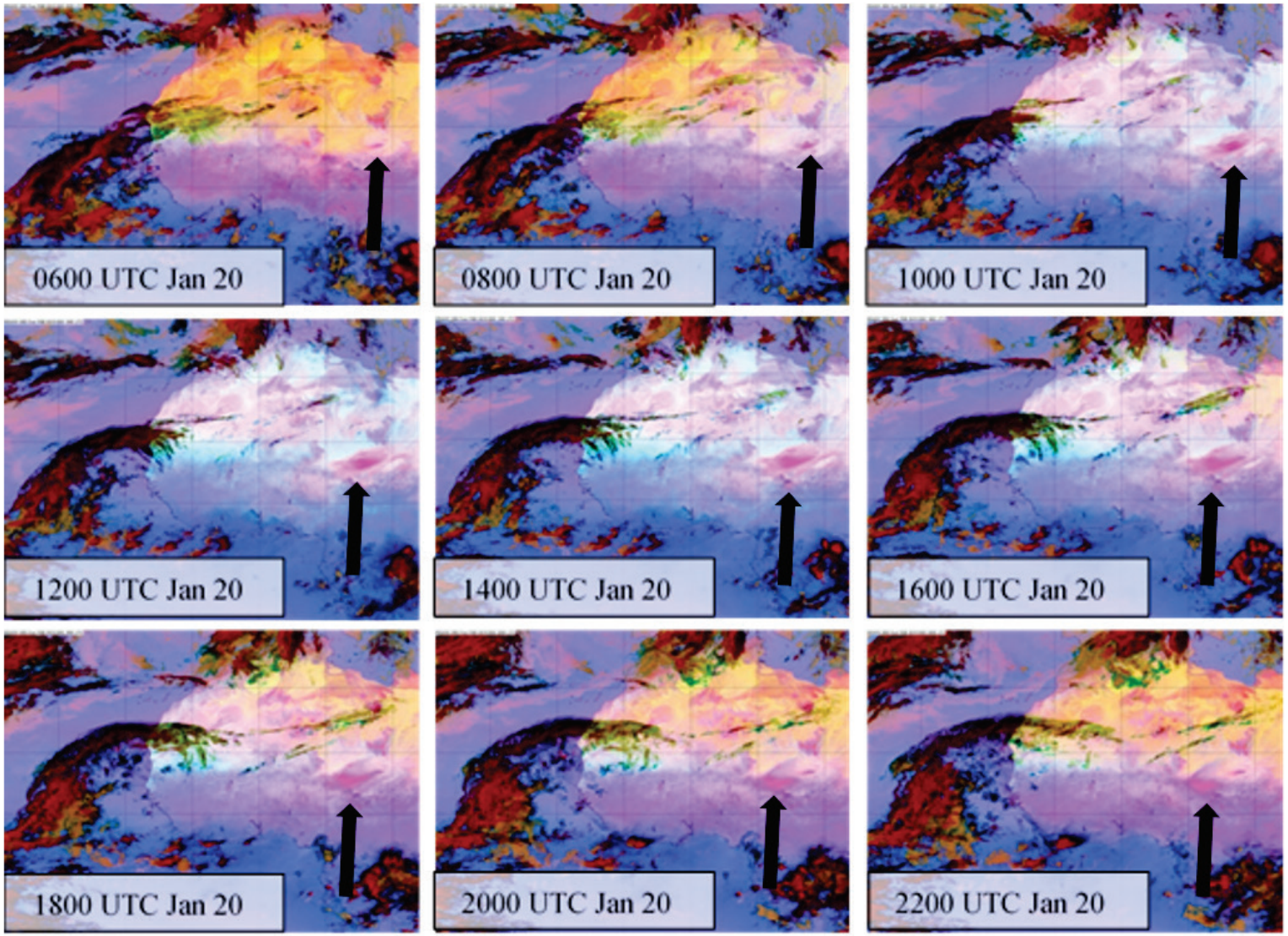

An AERONET station at Zinder Airport in Chad at 13.77°N and 8.99°E recorded a spike in AOD on 20 January when the dust plume passed over the area (Figure 16). The 440 nm AOD channel reached a level of approximately 2.5 at its highest point during the event. However, the only available AOD measurements from this site during this time frame were level 1 (unscreened) data. While cloud contamination could have made it into the measurements, no clouds were apparent in the MSG-SEVIRI imagery near this area. It is unclear why data managers removed this period from the quality-controlled data sets. A spike in AOD over the Bodélé Depression and locations to the southwest in the MODIS AOD product for 20 January is displayed in Figure 17.

Figure 16. Level 1 AERONET AOD at Zinder Airport in Zinder, Chad for January 2021.

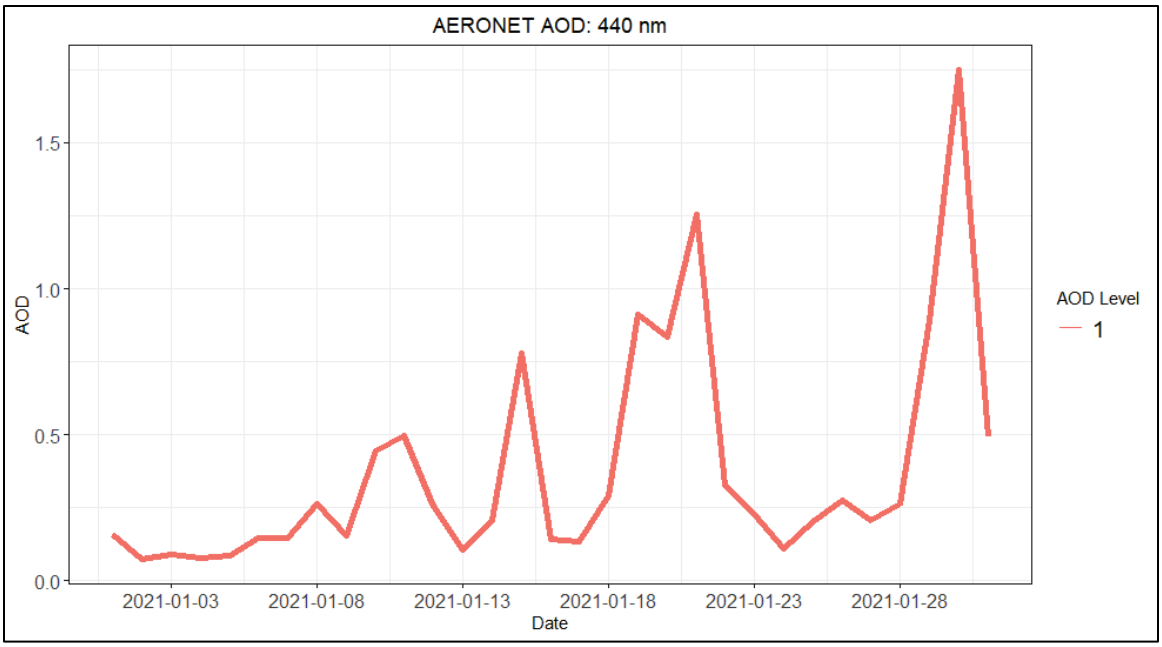

Figure 17. MODIS AOD for 20 January 2021. Note the large dust plume (circled) over the Bodélé Depression.

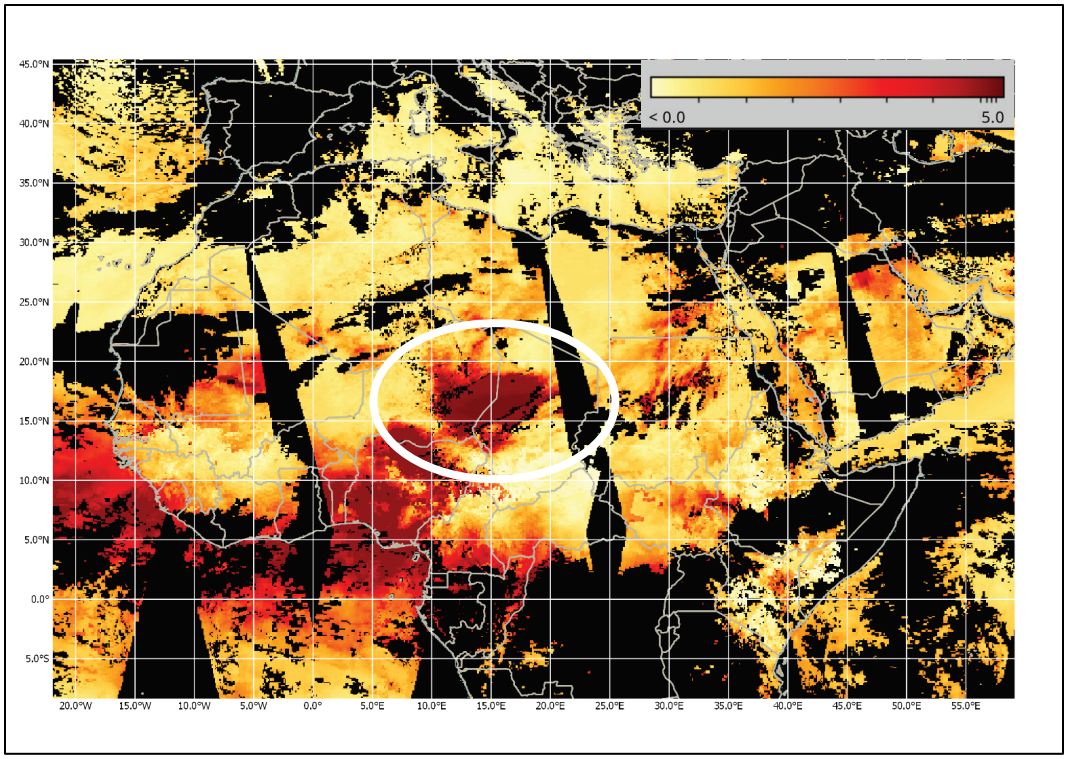

CALIPSO products for 1318–1332 UTC on 21 January of 532 nm total attenuated backscatter and aerosol subtype indicate that dust reached approximately 2.5 km into the atmosphere between 9°N–20°N and 7°E–11°E (Figure 18). The aerosol subtype product suggests that the aerosols in the shallow layer above the surface were primarily dust.

Figure 18. CALIPSO vertical profile products. Same as Figure 6 but for 20 January 2021, 1318–1332 UTC. Note the color of the orbit line associated with the transect is green here instead of pink.

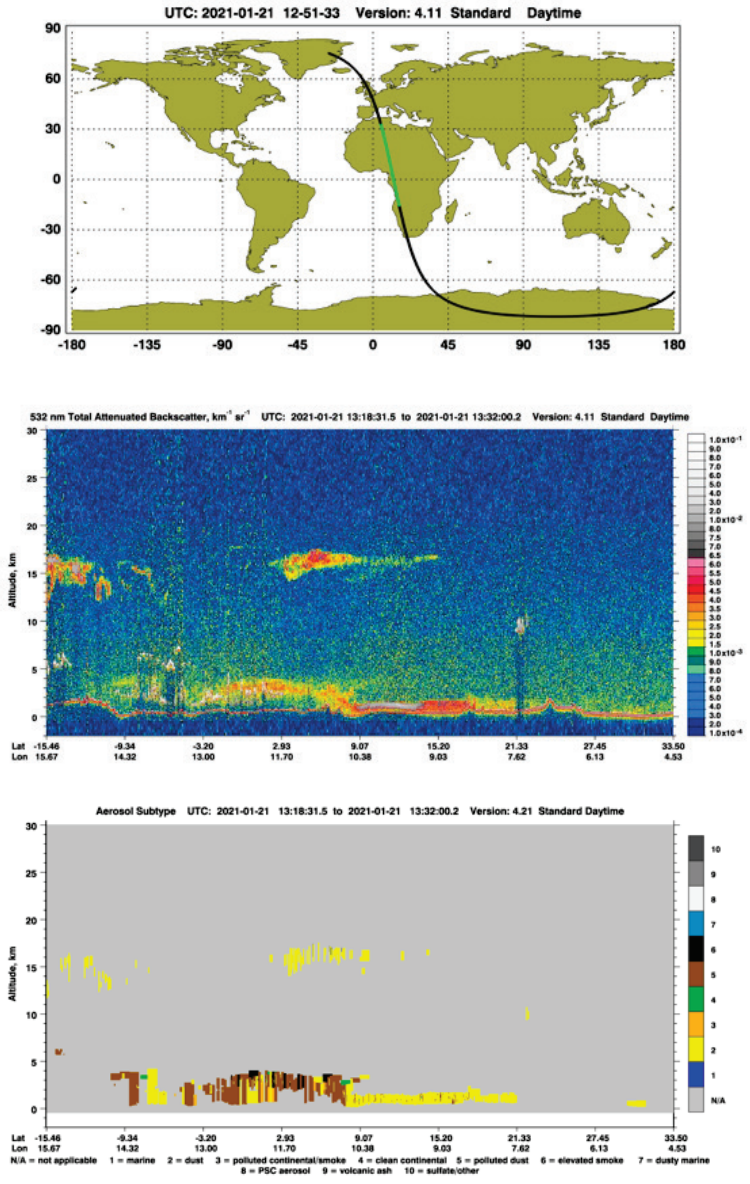

3.3 5–7 February 2021–Algeria and Morocco

3.3.1 Event overview

The third case study the researchers analyzed occurred near the northern border of Algeria and Morocco on 5 February 2021. Dust emissions began around 1200 UTC 5 February and persisted until approximately 0000 UTC 6 February. The event occurred when a deep trough swept in from the North Atlantic across Morocco and Algeria while a high-pressure ridge was

in place to the east over southeastern Algeria and Libya (Figure 19). This type of pattern has been linked to previous dust outbreaks over Algeria with transport into the central Mediterranean region (Barkan et al. 2005; Prospero et al. 2020; Middleton and Goudie 2001). Strong midlevel flow rapidly transported the high concentrations of dust northeastward into parts of Europe, including Spain, France, Switzerland, and Germany.

Figure 19. Dust emission forcing conditions of the 5–7 February 2021 dust storm in Algeria and Morocco. The blue H and red L surrounded by dashed lines represent the general location of strong high- and low-pressure systems, respectively. The area outlined by the black box represents the general dust source region, and the red arrow represents a region of strong winds. The area along the northern Algeria coastline circled in red is the Dar-El-Bedia sounding location.

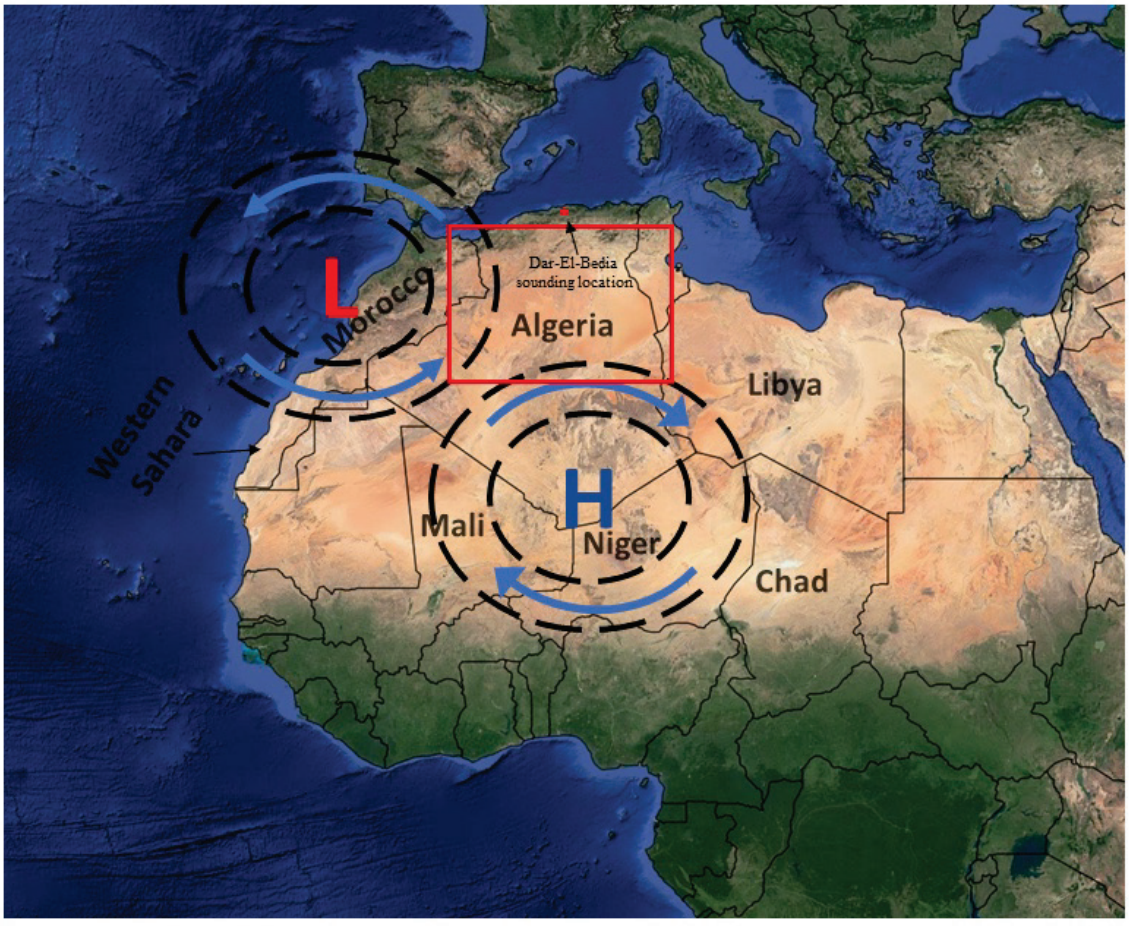

3.3.2 Synoptic overview

The Figure 20 600 hPa geopotential height and wind speed ERA5 analyses show a highly amplified wave-train pattern propagating across northwest Africa. Strong geopotential height falls approached northwest Africa from the west, with a sharp height gradient centered over Algeria on the 1200

UTC analysis for 5 and 6 February. As the trough approached, the ridge over Libya and Niger strengthened. The 600 hPa winds displayed in Figure 20 maxed out over Algeria and the Mediterranean Sea on the 1200 UTC 5 February analysis in areas where winds reached speeds of 45 ms^{-1}. The low-level jet displayed on the 850 hPa analysis (Figure 21), began at 1200 UTC 5 February with wind speeds that reached approximately 20 ms^{-1} over western Algeria. By 1200 UTC 6 February, the 850 hPa winds over central Algeria increased to approximately 25 ms^{-1}, and strong low-level winds were favorable for rapid northeastward transport of the dust plume. Figure 22 displays the evolution of 10 m winds for this event. The analysis valid for 1200 UTC 3 February and 4 February indicated relatively weak winds (<5 ms^{-1}) over the dust source region near the Morocco/Algeria border. An anticyclonic flow formed at the surface with strong northerly winds across Egypt and Sudan. Winds turned easterly along the southern side of the ridge across Chad and Niger, with southerly flow over Mali and Algeria. As the trough moving in from the west deepened over Western Sahara and Morocco, the high-pressure ridge intensified over north-central Africa. Winds also began to intensify over the dust source region, reaching >10 ms^{-1} through Mali and Algeria by 1200 UTC on 5 February. The axis of strong surface winds remained over Mali and Algeria through 6 February and shifted eastward to eastern Algeria and western Libya on 7 February. The 0000 UTC soundings on 5 and 6 February show the strong low-level southeasterly flow in Dar-El-Bedia as the trough passed over the area (Figure 23).

Figure 20. ERA5 reanalysis of 600 hPa wind speed (ms^{-1}; shaded), geopotential height (m; contoured), and wind barbs valid at 1200 UTC 3–7 February 2021. Note the propagation of strong midlevel winds across Morocco and Algeria.

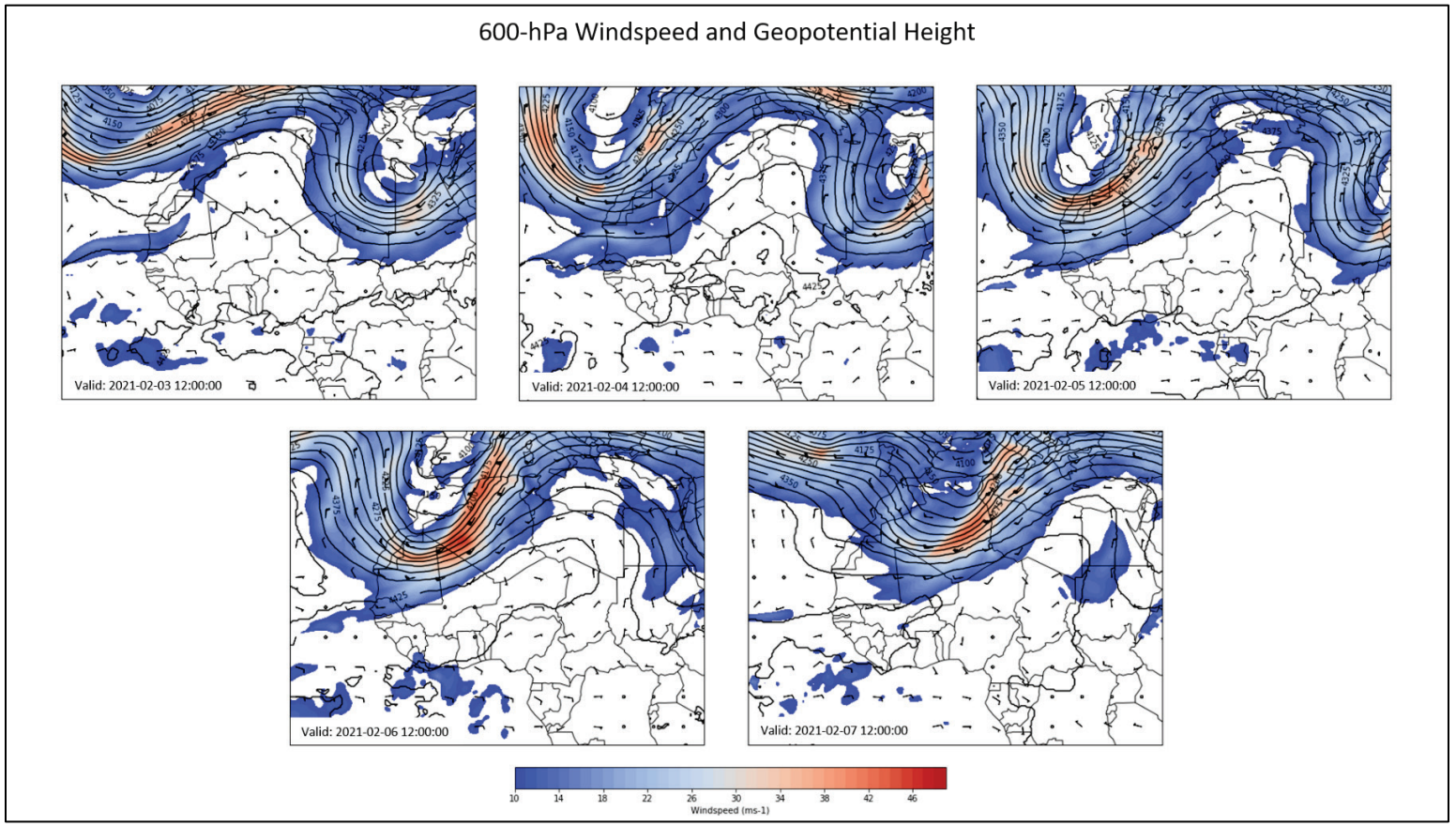

Figure 21. ERA5 reanalysis of 850-hPa wind speed (ms^{-1}; shaded) and wind barbs valid at 1200 UTC 3–6 February 2021. Note the strong low-level winds across Algeria and Morocco.

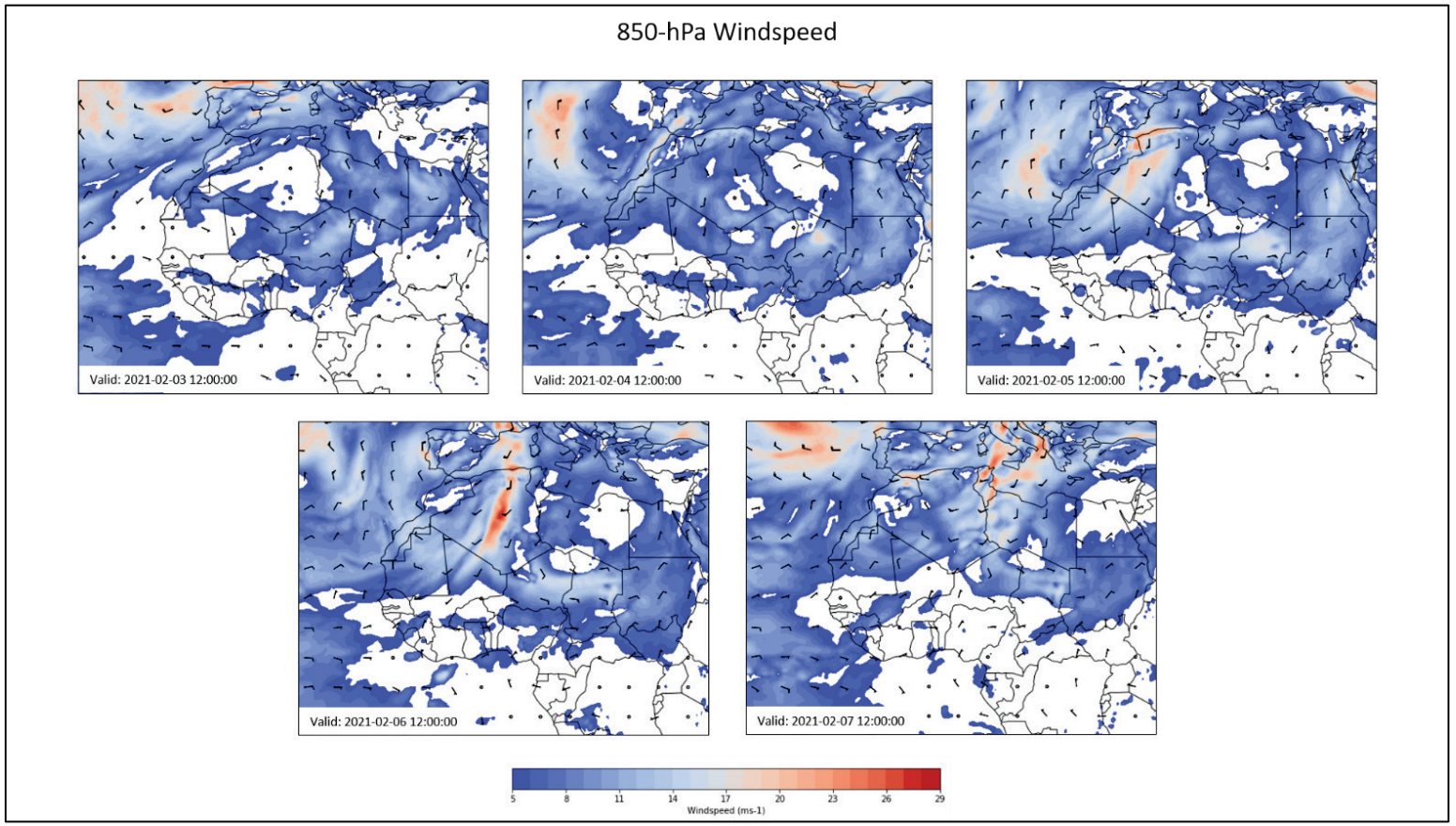

Figure 22. ERA5 Reanalysis of 10 m wind speed (ms^{-1}; shaded) and wind barbs valid at 1200 UTC 3–7 February 2021. Note the strong surface winds that develop near the Algeria and Morocco border.

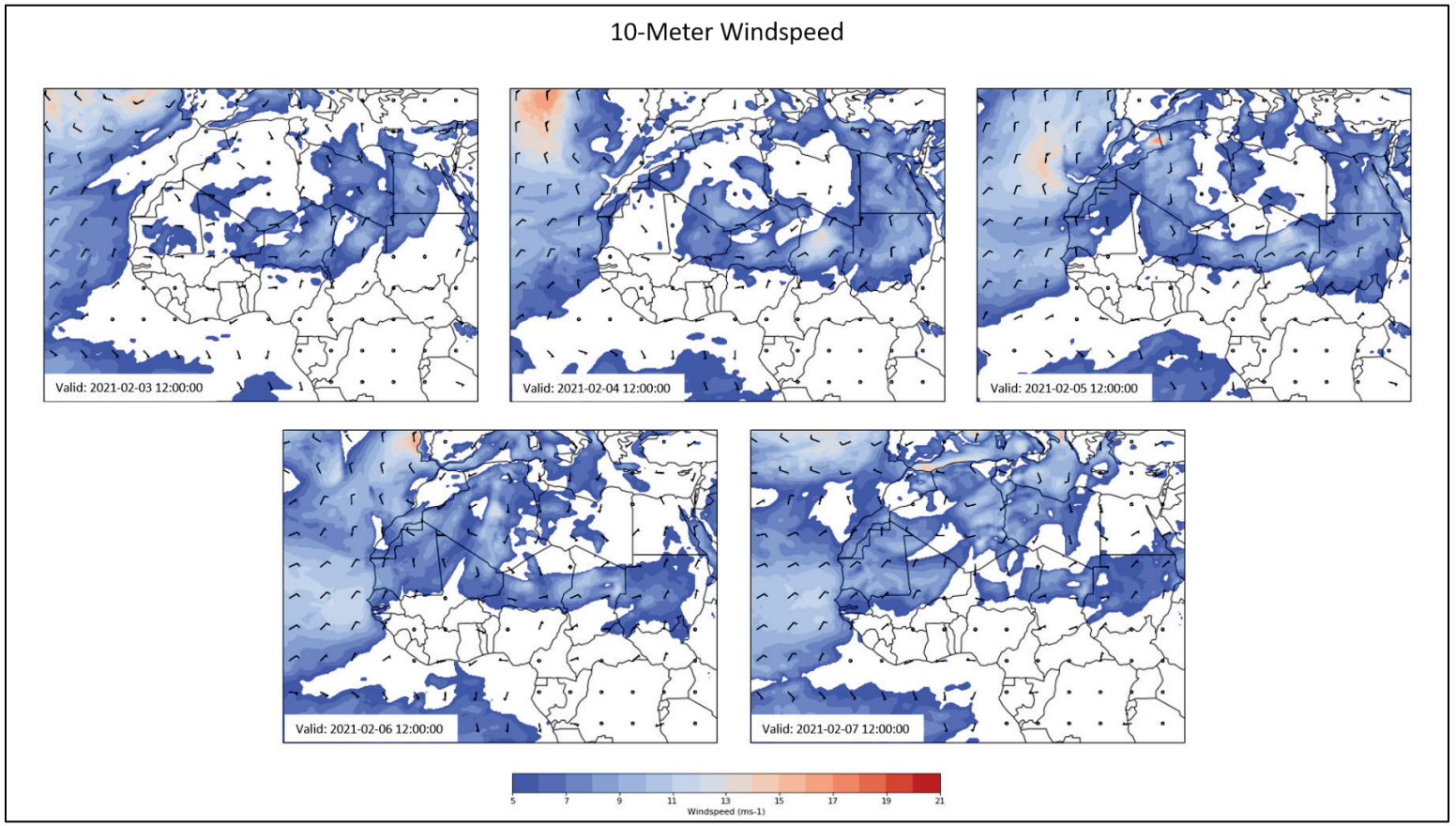

Figure 23. Upper-air sounding at Dar-El-Bedia at 0000 UTC 5 (left) and 6 (right) February 2021.

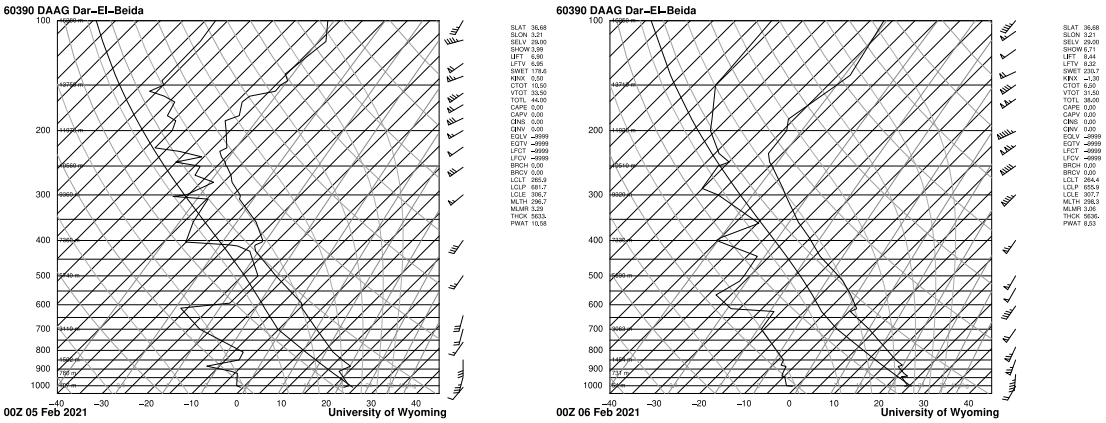

3.3.3 Dust storm evolution

Figure 24 shows the MSG-SEVIRI imagery for the dust event that began on 1200 UTC 5 February, with dust emission occurring until approximately 0000 UTC 6 February. The initiation of the event appears to closely coincide with a spike in the 10 m wind speed near the Algeria and Morocco border, where winds reached approximately 20 ms^{-1} (e.g., Figure 22). It appears that strong midlevel and low-level winds were brought down to the surface by convection just north of the Morocco coastline. A rapid spike in surface winds occurred at the Melilla weather observation station located 35.30°N, 2.94°W approximately 1100 UTC (Figure 25). Dust emission continued for much of the day, and the dust plume rapidly transported north across the Mediterranean Sea into parts of Europe by the strong low-level winds that were in place over the area. By the 0000 UTC analysis, dust emissions ceased, and the dust plume advected northward out of Algeria.

Figure 24. MSG-SEVIRI dust-enhanced imagery for 1200 UTC 5 February 2021–0400 UTC 6 February 2021, with arrows pointed at dust plume. Concentrated areas of pink and magenta colors generally indicate airborne dust, while areas of red or brown shading are generally thick clouds.

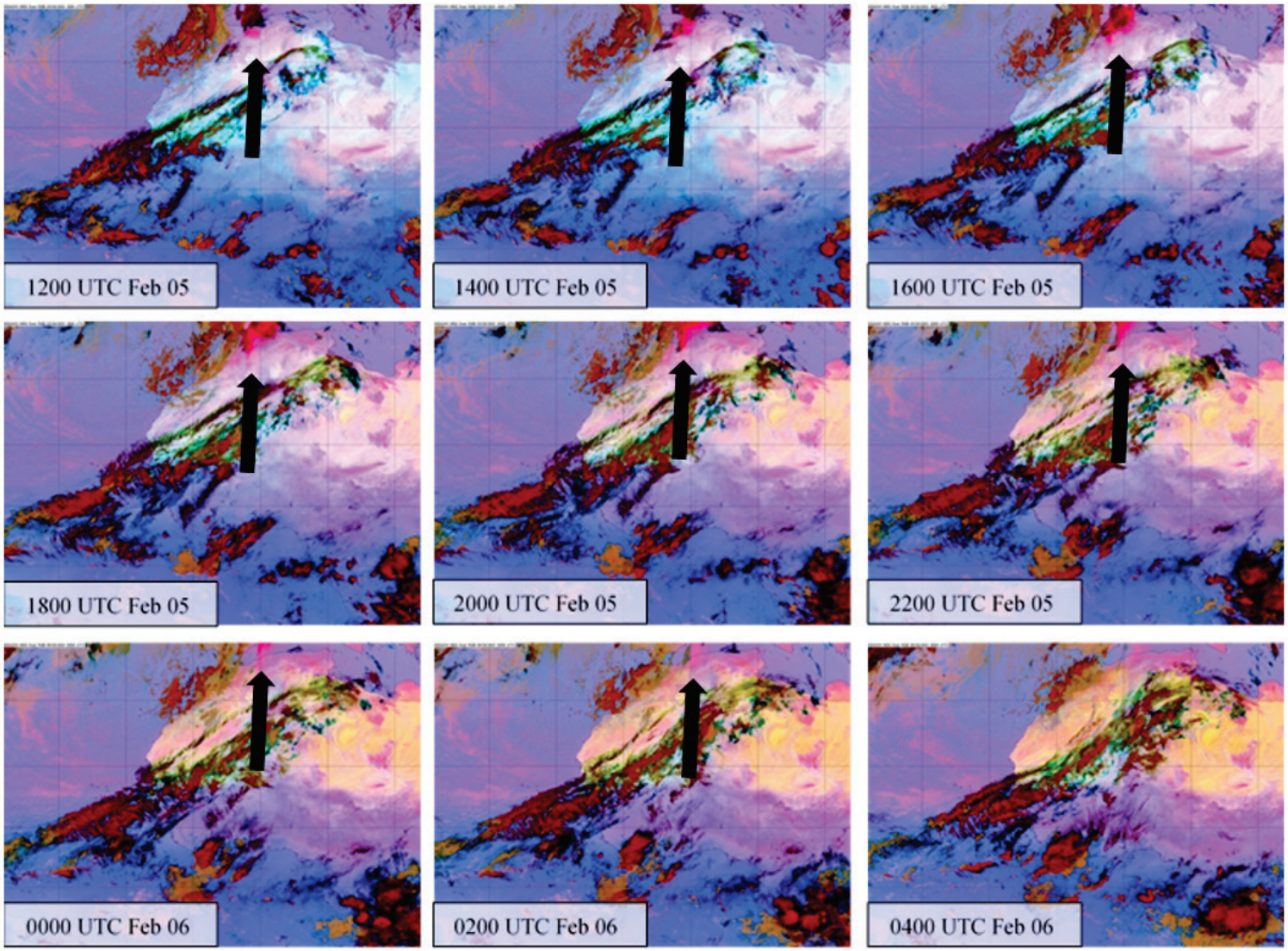

Figure 25. 5 February 2021 weather observations from the Melilla station at 35.30°N, 2.94°W in Morocco. Note the figure shows the station time in local time, which is UTC+1 hour.

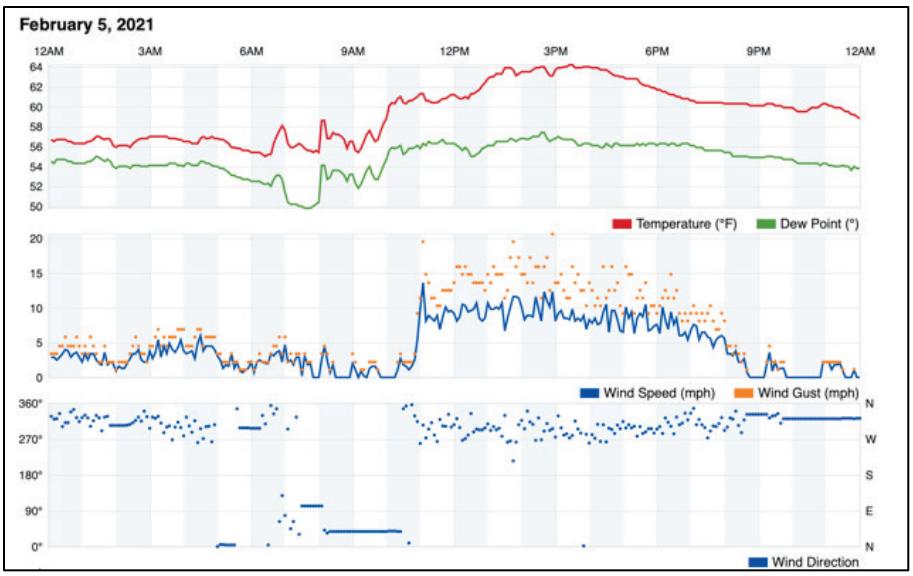

An AERONET station in Medenine, Tunisia (33.5°N, 10.64°E), recorded a spike in AOD on 6 February (Figure 26), reaching approximately 1.25 at the peak of the event for the 440 nm wavelength. Since this event occurred on the fringes of a trough associated with a frontal boundary, the effect of cloud contamination in the level 1 AOD data set is apparent. Figure 27 shows the dust plume advecting northward from Algeria on 6 February in the MODIS AOD product.

Figure 26. Aerosol optical depth in Medenine, Tunisia for February 2021, including the level 1 unscreened (and level 1.5 cloud-screened data sets.

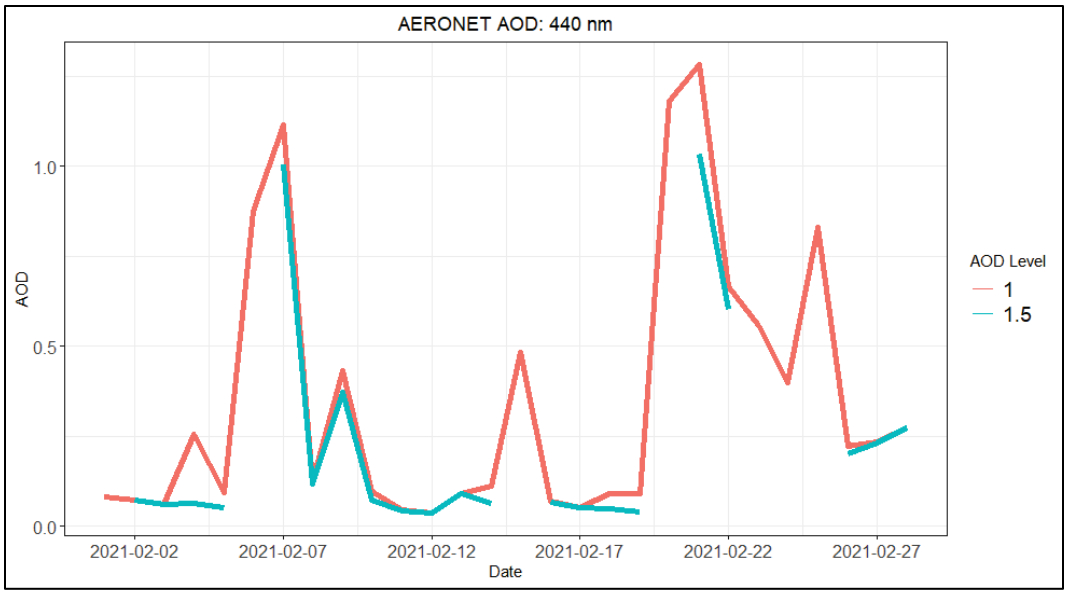

Figure 27. MODIS AOD for 6 February 2021 with dust plume circled.

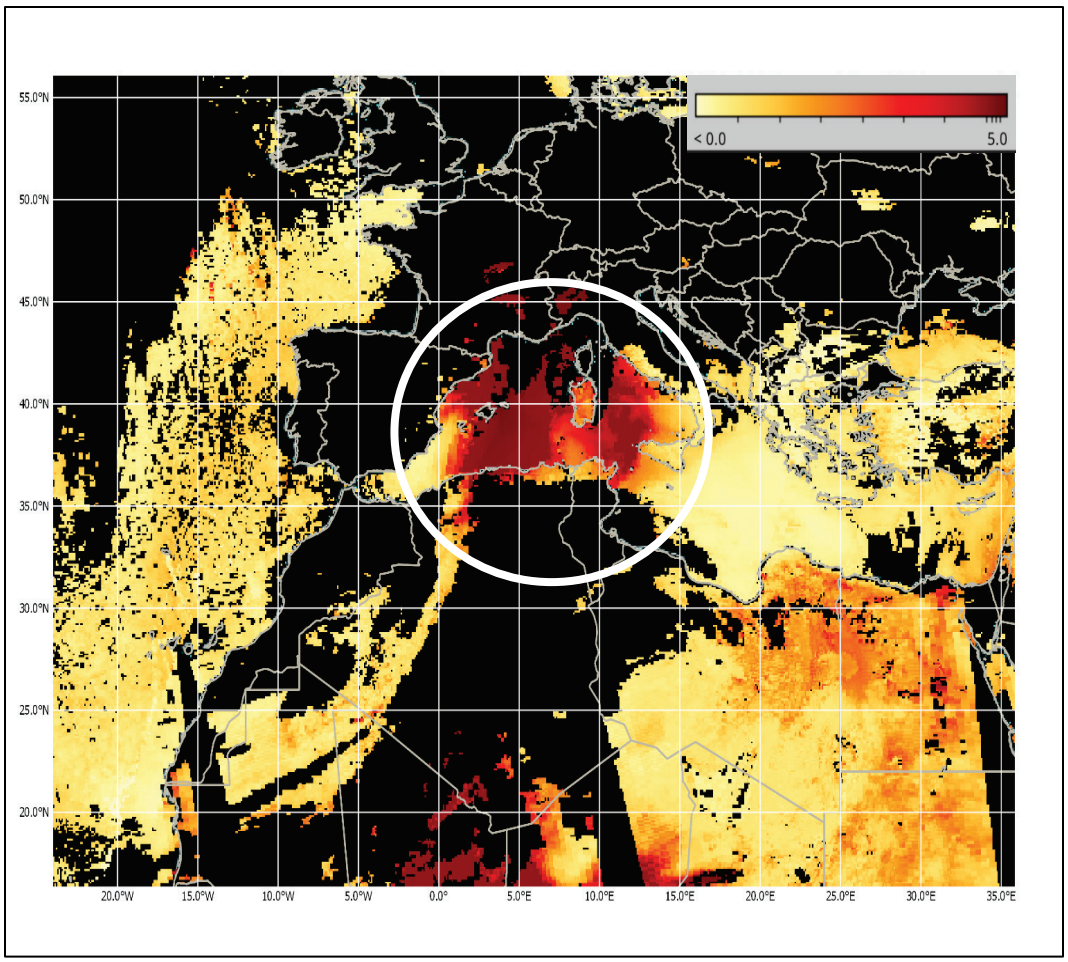

CALIPSO products for 1333–1347 UTC on 6 February of 532 nm total attenuated backscatter and aerosol subtype indicate that dust reached approximately 2.5 km into the atmosphere between 32°N–38°N and 0°E–2°E (Figure 28). The aerosol subtype product suggests that the aerosols in the shallow layer above the surface were primarily dust.

Figure 28. CALIPSO vertical profile products. Same as Figure 7 but for 6 February 2021, 1333–1347 UTC. Note the color of the orbit line associated with the transect is green here instead of pink.

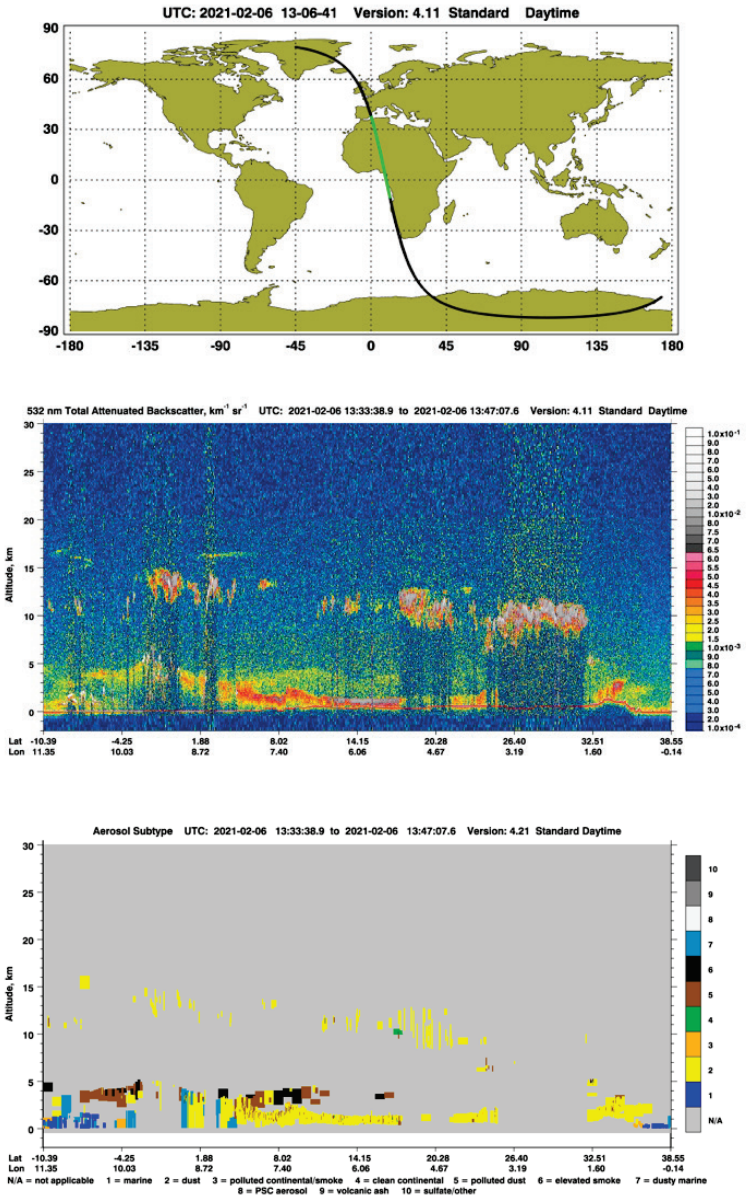

3.4 20–24 February 2017–East Algeria and the Iberian Peninsula

3.4.1 Event overview

The fourth case study the researchers analyzed initiated over northwestern Algeria and Morocco and transported dust into the Iberian Peninsula from 20–24 February 2017. Anticyclonic high-pressure circulation over eastern Algeria and Libya and a cutoff low-pressure system to its west over

Morocco set the conditions for the dust storm with an enhanced southerly flow between the two circulations (Figure 29). The regional orographic features of northern Algeria and Morocco, combined with the strong low-level flow, resulted in the development of a mesoscale cyclonic vortex (MCV)* that brought strong surface winds across the dust source region of northwestern Algeria and Morocco. Previous analyses of this dust event indicate that extreme amounts of dust with AODs >2.0 were transported from Algeria into the Iberian Peninsula over the duration of the storm (Couto et al. 2021; Fernández et al. 2019).

Figure 29. Environmental conditions associated with or responsible for dust emissions during the 20–24 February 2017 dust storm in Algeria and Morocco. The blue H and red L surrounded by dashed lines represent the general location of strong high- and low-pressure systems, respectively. The area outlined by the black box represents the general dust source region, and the red arrow represents a region of strong winds.

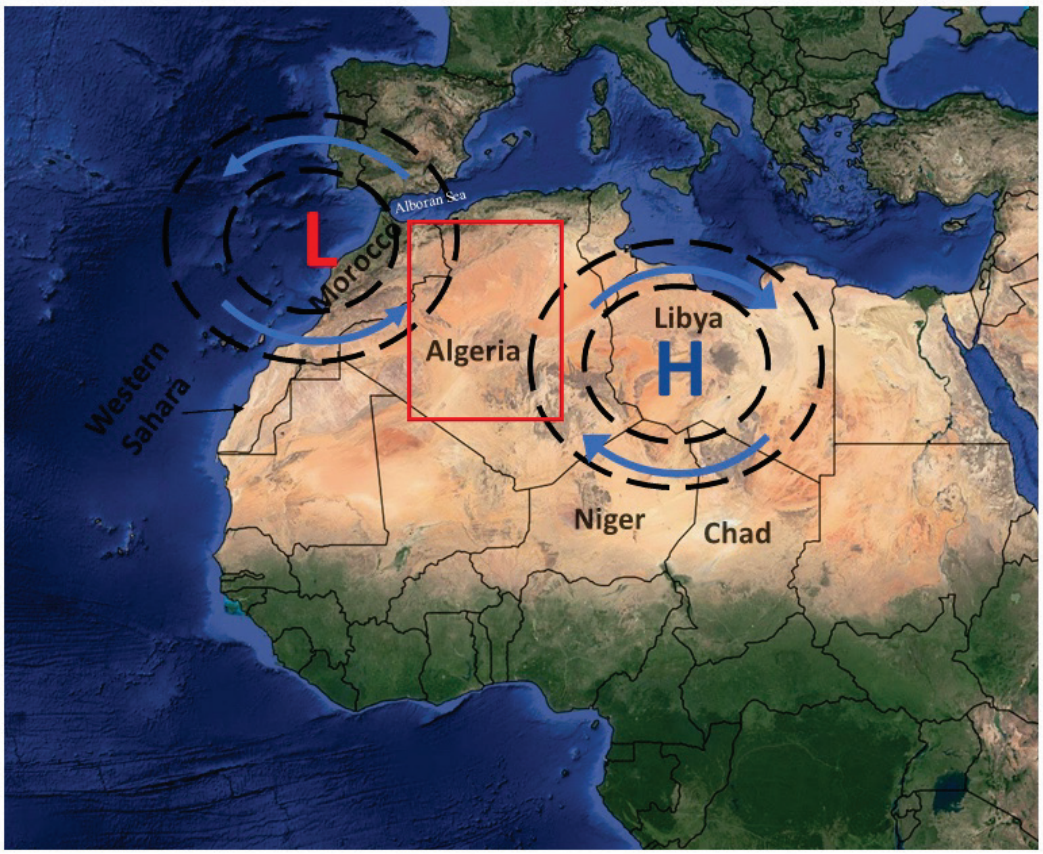

3.4.2 Synoptic overview

Figure 30 shows the midlevel synoptic evolution of this event through the 600 hPa geopotential height analysis. The analysis valid at 1200 UTC 19 February displays a ridge over the Atlantic Ocean, northwest of the African coastline, and a cutoff low over Morocco. To the east of the cutoff low, there was a high-pressure ridge centered over Algeria and Libya. This pattern remained relatively stationary through the 1200 UTC 23 February analysis. While the low-pressure center over Morocco expanded south and eastward between 19 and 24 February, the high-pressure ridge to the east intensified. As a result, the pressure gradient between these two circulations generated strong midlevel winds across portions of eastern Algeria. The 600 hPa wind speed analysis in Figure 30 shows 600 hPa enhanced winds from the northern tip of Mali to western Algeria. The axis of strongest winds on the eastern side of the low remained stationary through 23 February but fluctuated in speed, with the strongest winds reaching approximately 35 ms^{-1}. By the 1200 UTC February 24 analysis, the axis of strongest winds had propagated over eastern Algeria and the Mediterranean Sea.

The 850 hPa wind analysis in Figure 31, valid for 1200 UTC 19–24 February, displays persistent low-level winds conducive to dust transport across much of Algeria. The winds on the eastern side of the cutoff low remained at speeds approximately 25 ms^{-1} throughout the analysis. The strong 850 hPa winds resulted in the development of a MCV, as indicated by the strong 10 m wind circulation over Morocco in Figure 32. Strong surface winds persisted across Algeria from 19 February until 23 February, with the strongest winds (>20 ms^{-1}) in the 10 m wind speed analysis occurring just along the northern Algeria coastline on the north side of the MCV. On the 24 February analysis, strong surface winds associated with the MCV across Algeria subsided.

Figure 30. ERA5 reanalysis of 600-hPa wind speed (ms^{-1}; shaded), geopotential height (m; contoured), and wind barbs valid at 1200 UTC 20–24 February 2017. Strong midlevel winds are apparent along the eastern side of the low-pressure center that propagates over Morocco and Algeria.

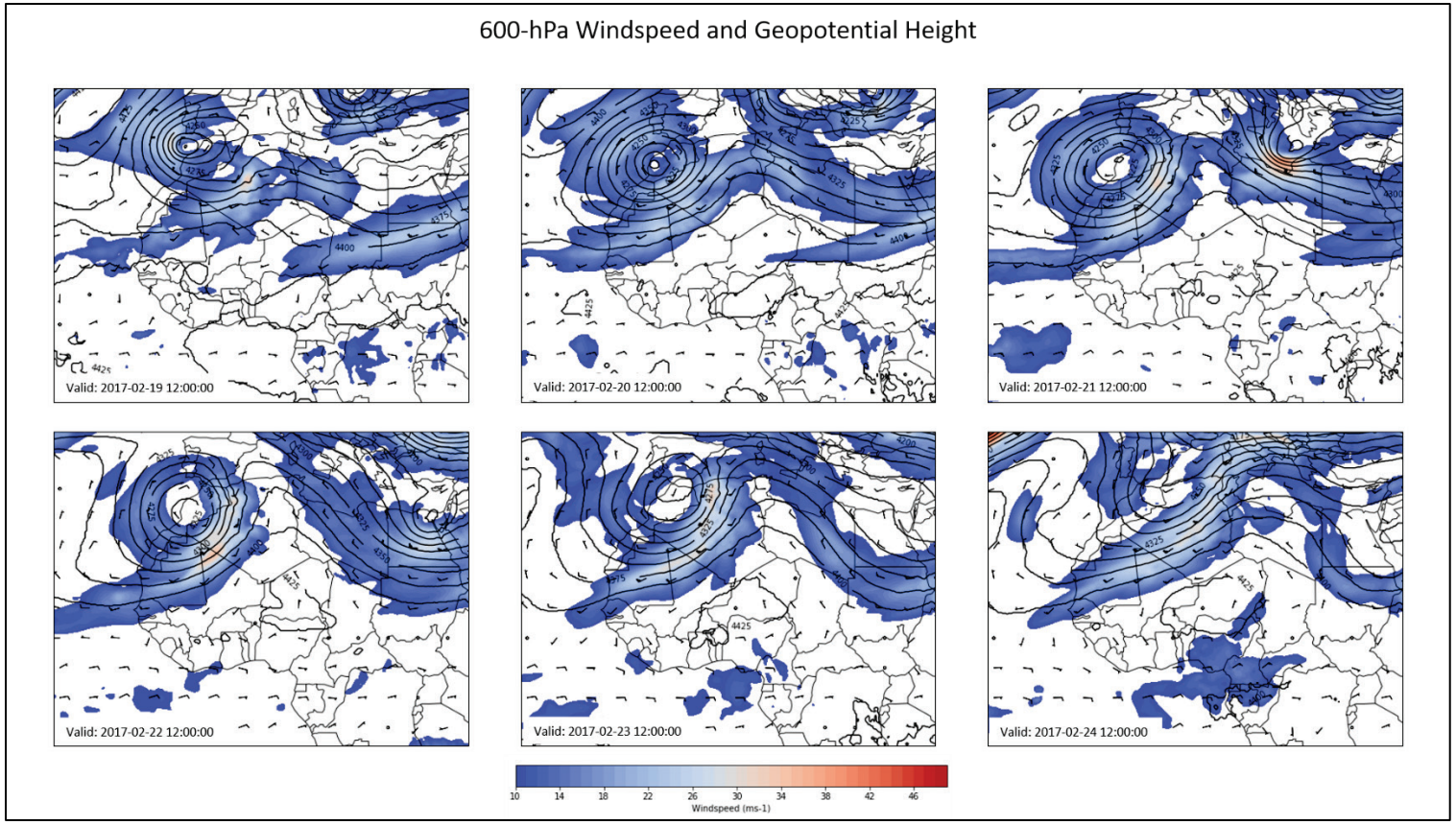

Figure 31. ERA5 reanalysis of 850 hPa wind speed (ms^{-1}; shaded) and wind barbs valid at 1200 UTC 20–24 February 2017. Note the strong low-level winds that occur over Algeria throughout the event.

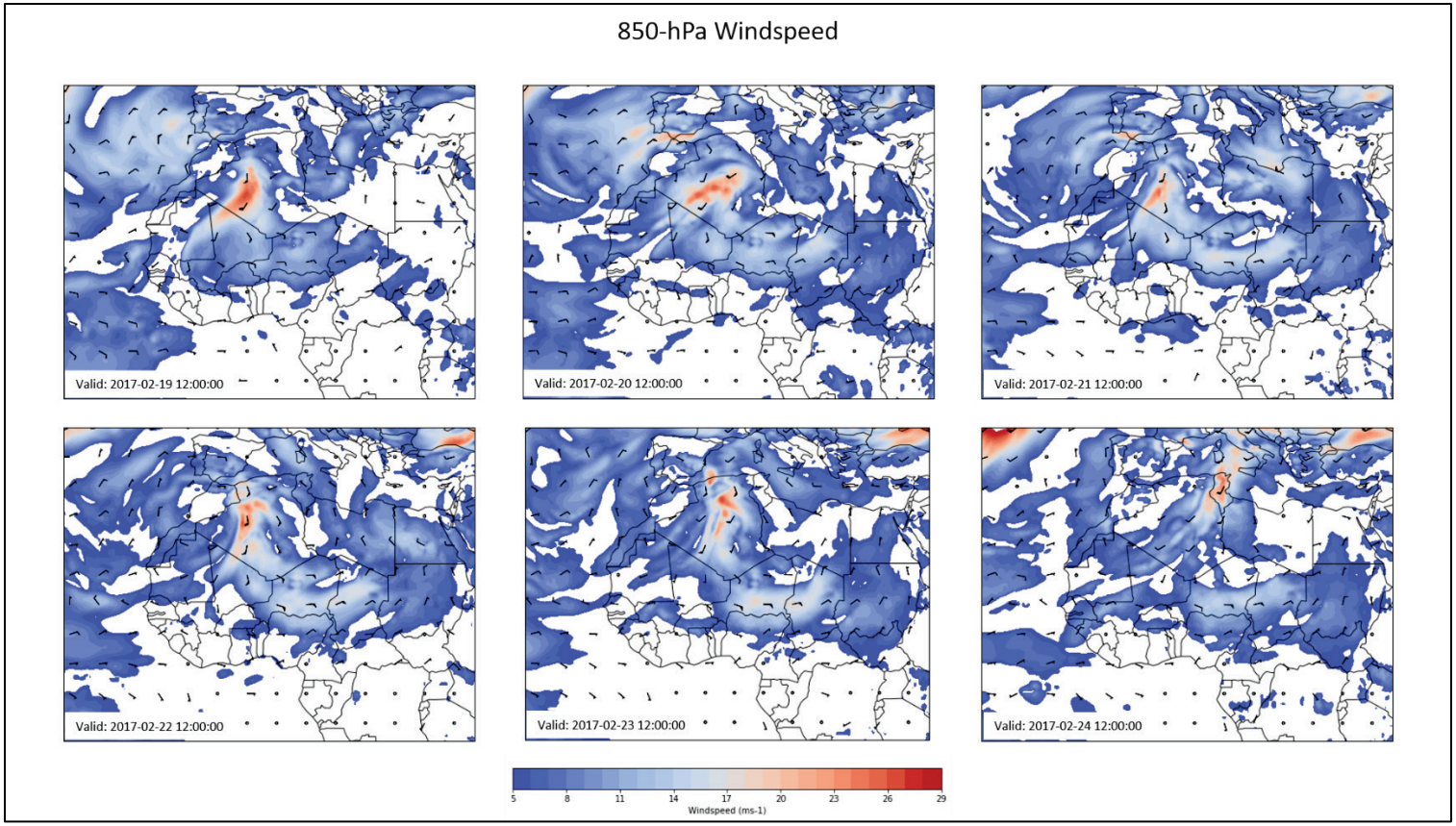

Figure 32. ERA5 Reanalysis of 10 m wind speed (ms^{-1}; shaded) and wind barbs valid at 1200 UTC 19–24 February 2017. Note the strong surface winds that develop near the Algeria and Morocco border.

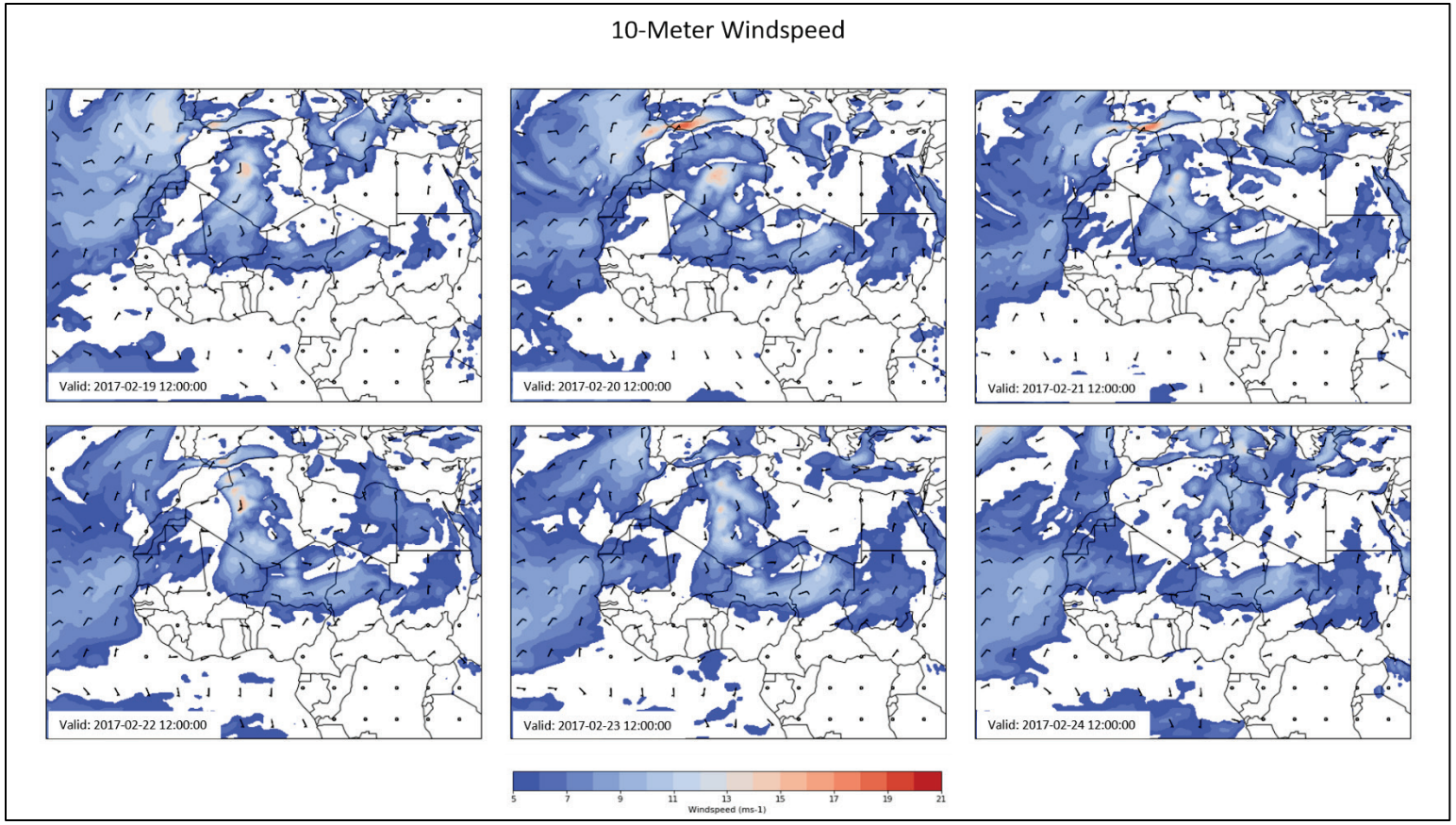

3.4.3 Dust storm evolution

Figure 33 illustrates the evolution of the dust storm with MSG-SEVIRI imagery from 19–24 February. The 1200 UTC image from 19 February shows a large area of cloud cover with the approaching low-pressure trough across southern Portugal, Spain, northern Morocco, and Algeria. An MCV was also located just off the western coastline of Portugal and Morocco. Though the area is relatively cloud obscured, the MCV appears to be generating dust emissions in Morocco. In the 1200 UTC 20 February image, the MCV moves eastward over northwestern Morocco, with the dust plume wrapping into the low-pressure circulation across Algeria, Morocco, and the Alboran Sea. The spiraling pattern of the dust plume across these regions continued through 1200 UTC 21 February. By 1200 UTC 22 February, the large dust plume advected northward across Algeria and Morocco into Spain and Portugal. Note the apparent dust plume in Figure 33 aligns with the area of strong 10 m winds in Figure 32.

Figure 33. MSG-SEVIRI dust-enhanced imagery for 1200 UTC 19–24 February 2017. Concentrated areas of pink and magenta colors generally indicate airborne dust, while areas of red or brown shading are generally thick clouds.

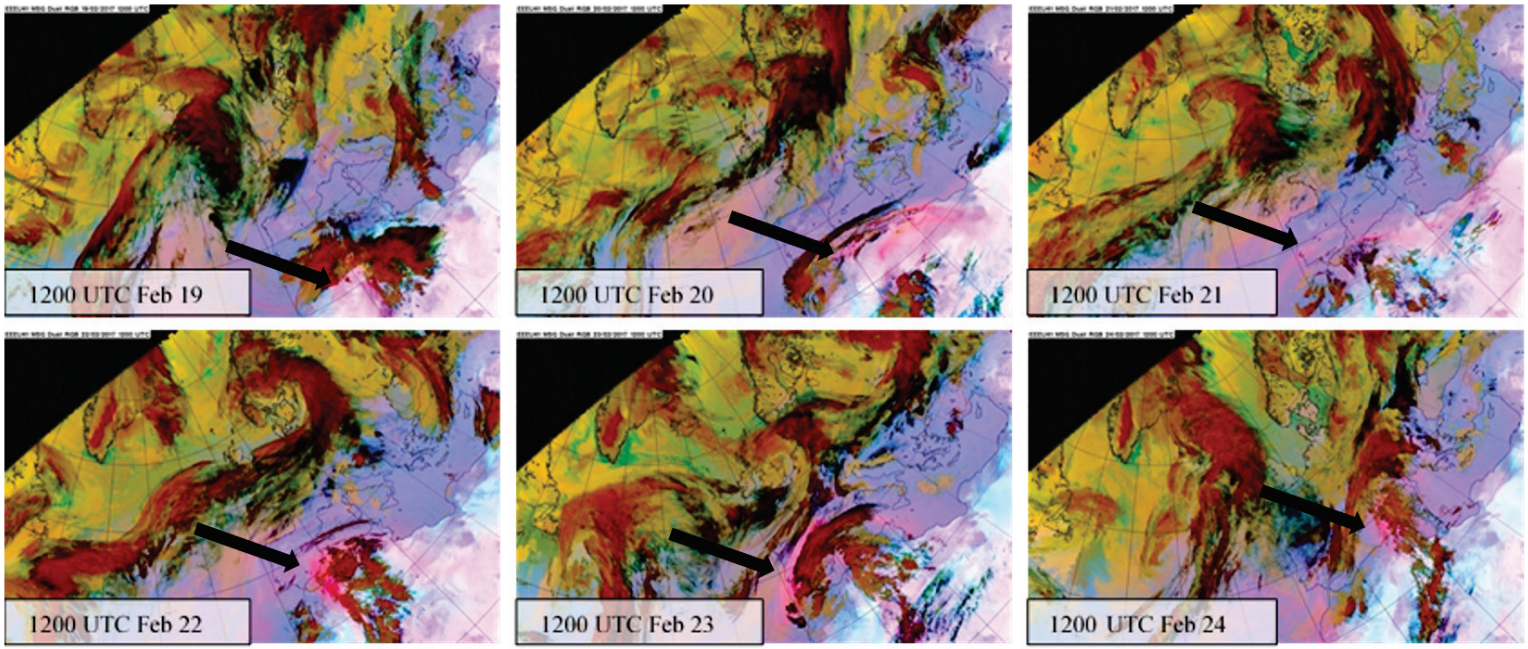

CALIPSO products for 0213–0226 UTC on 22 February of 532 nm total attenuated backscatter and aerosol subtype show the dust plume over Algeria and the Iberian Peninsula between 25°N–40°N and 0°E–5°W (Figure 34). A large plume of dust can also be seen advecting from Algeria into the Iberian Peninsula in the 22 February MODIS AOD product (Figure 35). By 23 February, the AERONET station at 37.09°N and 2.36°W in Tabernas, Spain measured an AOD of approximately 0.55 in the level 1.5 data set (Figure 36). These patterns align with the MSG-SEVIRI imagery (Figure 33), which suggests the majority of the dust plume had moved out of northern Algeria across the Mediterranean Sea by 1200 UTC 24 February.

Figure 34. CALIPSO vertical profile products. Same as Figure 6 but for 22 February 2017, 0213–0226 UTC. Note the color of the orbit line associated with the transect is royal blue here instead of pink.

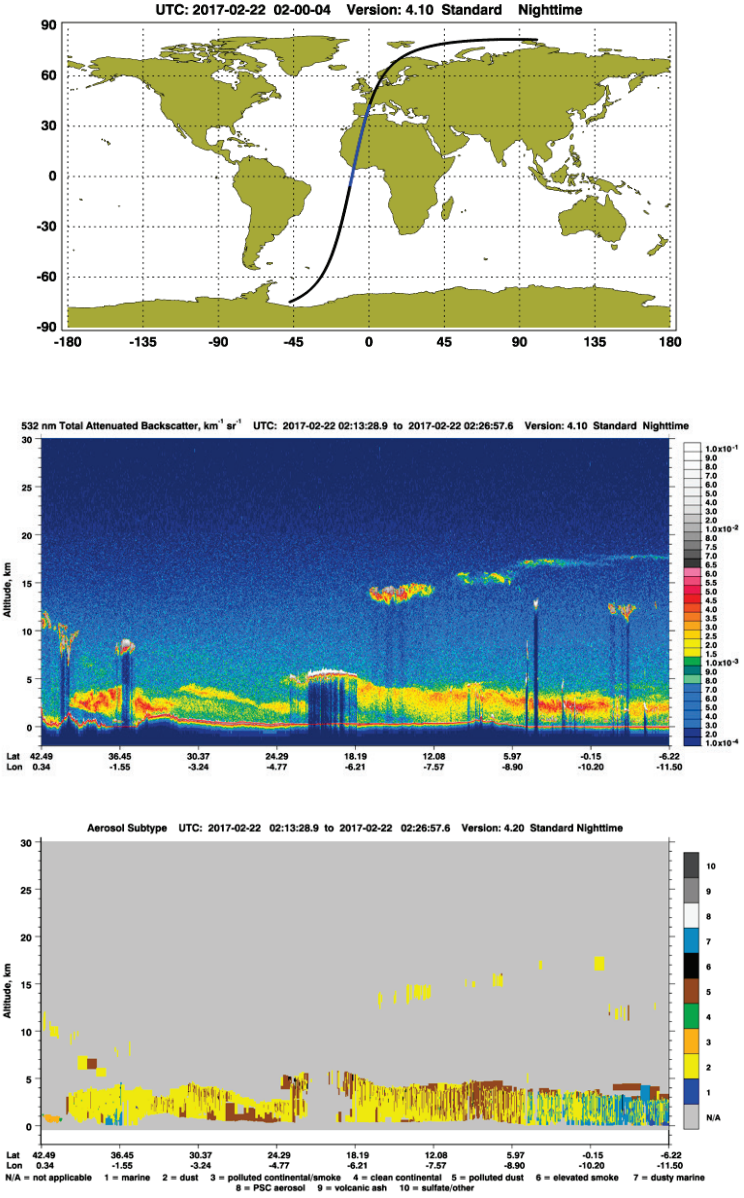

Figure 35. MODIS AOD for 22 February 2017.

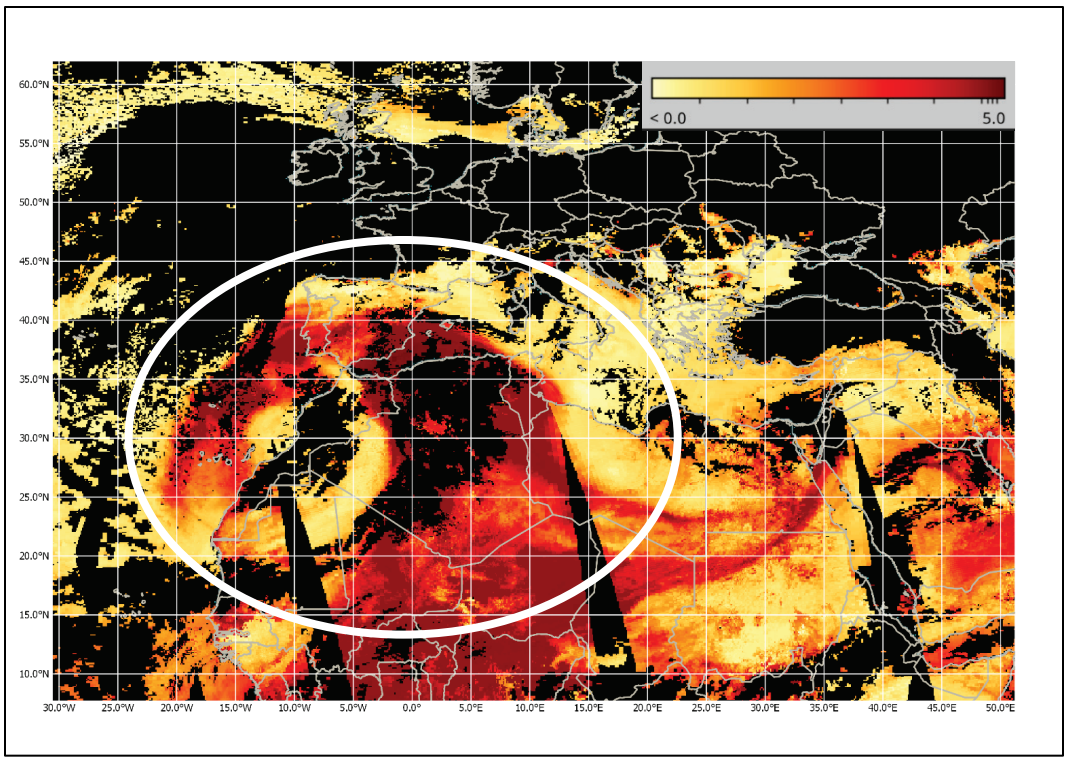

Figure 36. Aerosol optical depth at Tabernas, Spain for February 2017, including the level 1 unscreened, level 1.5 cloud-screened, and level 2.0 data sets. A peak of approximately 0.55 occurs in the in cloud-screened and fully quality-controlled AOD measurements at this AERONET station location on 23 February.

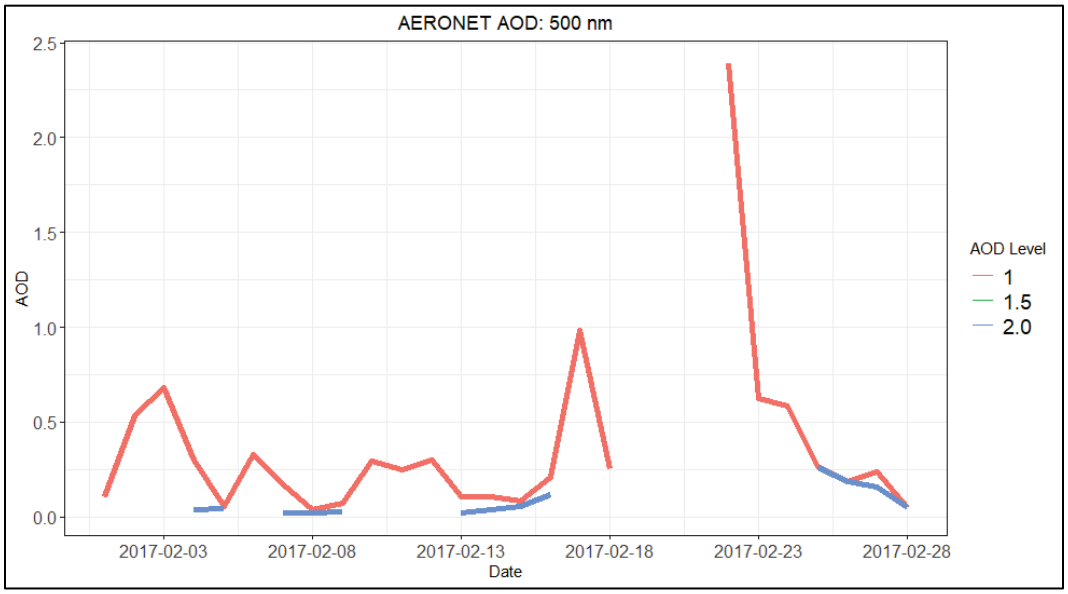

4 Conclusion

4.1 Summary

The researchers performed an in-depth meteorological analysis of four dust storm events in the North Africa region. The general forcing conditions were analyzed using ERA5 reanalysis data, upper-air sounding data, and MSG-SEVIRI satellite imagery. These assessments highlighted the synoptic and mesoscale characteristics associated with each event, focusing on how the larger-scale and regional-scale atmospheric features influenced dust emissions. The researchers also analyzed the evolution of dust plumes related to each event by using AERONET AOD data, MODIS AOD data, CALIPSO products, and MSG-SEVIRI imagery. In addition to reanalysis, satellite retrievals, and observational data, the analyses were supplemented with findings from previously published literature when available. By providing case study reference material, this report will guide future forecast model validation efforts.

4.2 Future work

Forecasters can use these analyses alongside previous studies that have investigated the effects of Saharan dust events on downstream air quality, sea surface temperatures, precipitation patterns, and tropical cyclone activity (Francis et al. 2022; Pu and Jin 2021). The forcing mechanisms analyzed in the four case studies transported dust well beyond the North Africa dust source regions, reaching portions of Europe, the Atlantic Ocean, Caribbean Sea, and the southeastern US. This report could be used as a guide to further investigate the effects of the dust plumes on weather patterns downstream of the dust source regions analyzed. Supporting this need for expanding our research downstream, a recent study found that the Godzilla dust event of June 2020 could have contributed to an increase in tropical cyclone activity in the Atlantic Basin due to a net warming of sea surface and air temperatures over the Atlantic Ocean (Francis et al. 2022). This discovery opposes other previous studies which have linked Saharan dust to a decrease in tropical cyclone activity. It is reasonable to suspect that the net warming caused by the Saharan dust could have been a contributing factor in this record-breaking hurricane season where 30 named tropical cyclones (with maximum sustained winds of 39 mph or greater), 14 hurricanes, and 7 major hurricanes were produced (noaa.gov). Another recent study by Francis et al. 2022 investigated the link between

atmospheric rivers and dust events that extend into portions of Europe, including the 5–7 February 2021 case study that was analyzed in our work. Their findings suggested that atmospheric rivers often influence dust transport from North Africa towards Europe and that these types of dust events could potentially lead to a decrease in snowpack downstream.

The link between atmospheric rivers that are associated with momentum transfer from jet streaks to the surface and the dust events described in this report, as well as other significant dust events, should be analyzed in future work. Linking these weather phenomena to the emission and transport of dust could improve short and long-range forecasting techniques and help forecasters predict the impacts they will have on atmospheric and hydrologic conditions downstream. Further analysis of this type will provide a better understanding of how dust events will affect human health, communication, travel, agriculture, and military operations across the globe.

References

Banks, J. R., and H. E. Brindley. 2013. "Evaluation of MSG-SEVIRI Mineral Dust Retrieval Products over North Africa and the Middle East." *Remote Sensing of Environment* 128: 58–73. https://doi.org/10.1016/j.rse.2012.07.017.

Barkan, J., P. Alpert, H. Kutiel, and P. Kishcha. 2005. "Synoptics of Dust Transportation Days from Africa toward Italy and Central Europe." *Journal of Geophysical Research* 110:D07208. doi:10.1029/2004JD005222.

Barlett, K. S. 2004. *Dust Storm Forecasting for Al Udeid Ad.* Qatar: An Empirical Analysis, Masters thesis. Air Univ., Ohio.

Brindley, H., P. Knippertz, C. Ryder, and I. Ashpole. 2012 A "Critical Evaluation of the Ability of the Spinning Enhanced Visible and Infrared Imager (SEVIRI) Thermal Infrared Red-Green-Blue Rendering to Identify Dust Events: Theoretical Analysis." *J. Geophys. Res. Atmos.*117:D07201.

Couto, F., E. Cardoso, M. Costa, R. Salgado, J. Guerrero-Rascado, and V. Salgueiro. 2021. "How a Mesoscale Cyclonic Vortex over Sahara Leads to a Dust Outbreak in South-Western Iberia." *Journal of Atmospheric Research* 249:1–13. https://doi.org/10.1016/j.atmosres.2020.105302.

Crook, J. 2009. *Climate Analysis and Long Range Forecasting of Dust Storms in Iraq."* Masters thesis. Naval Postgraduate School, Monterey, CA.

Engelstaedter, S., I. Tegen, and R. Washington. 2006. "North African Dust Emissions and Transport." *Earth Science Review* 79:73–100. https://doi.org/10.1016/j.earscirev.2006.06.004.

Fernández, A. J., M. Sicard, M. J. Costa, J. L. Guerrero-Rascado, J. L. Gómez-Amo, F. Molero, R. Barragán, et al. 2019. "Extreme, Wintertime Saharan Dust Intrusion in the Iberian Peninsula: Lidar Monitoring and Evaluation of Dust Forecast Models during the February 2017 Event." *Atmospheric Research* 228:223–241, 10.1016/j.atmosres.2019.06.007.

Francis, D., R. Fonseca, N. Nelli, D. Bozkurt, G. Picard, and Bin Guan. 2022. "Atmospheric Rivers Drive Exceptional Saharan Dust Transport towards Europe." *Atmospheric Research* 266. https://doi.org/10.1016/j.atmosres.2021.105959.

Francis, D., N. Nelli, R. Fonseca, M. Weston, C. Flamant, and C. Cherif. 2021. "The Dust Load and Radiative Impact Associated with the June 2020 Historical Saharan Dust Storm." *Atmos. Environ.* 268(2021): 118808. ISSN 1352-2310 https://doi.org/10.1016/j.atmosenv.2021.118808.

He, Y., and F. Yi, 2015. "Dust Aerosols Detected Using a Ground-Based Polarization Lidar and CALIPSO over Wuhan (30.5° N, 114.4° E), China." *Advanced Meteorology* 2015:536762.

Hersbach, H., B. Bell, P. Berrisford, S. Hirahara, A. Horányi, J. Muñoz-Sabater, J. Nicolas, et al. 2020. The Era5 Global Reanalysis, *Q." J. Royal Meteorological Society* 146:730. https://doi.org/10.1002/qj.3803.

Holben, B., N. 2001. "An Emerging Ground-Based Aerosol Climatology: Aerosol Optical Depth from AERONET." *Journal of Geophysical Research* 106:12067–12097.

Knippertz, P., and M. C. Todd. 2012. "Mineral Dust Aerosols over the Sahara: Meteorological Controls on Emission and Transport and Implications for Modeling, *Rev." Geophys*. 50:RG1007. doi:10.1029/2011RG000362.

LeGrand, S., and M. Brooks. 2018. "*Sensitivity of Unified Model Dust Simulations to the ERDC-Geo Surface Erodibility Parameterization*. White Paper. Vicksburg, MS: US Army Engineer Research and Development Center.

Levy, R. C., S. Mattoo, L. A. Munchak, L. A. Remer, A. M. Sayer, and F. Patadia. 2013. "The Collection 6 MODIS Aerosol Products over Land and Ocean." *Atmospheric Measurement Techniques* 6:2989–3034.

Li, J., E. Garshick, S. Huang, and P. Koutrakis. 2021. "Impacts of El Niño-Southern Oscillation on Surface Dust Levels across the World during 1982–2019." *The Science of the Total Environment* 769:144566. https://doi.org/10.1016/j.scitotenv.2020.144566.

Liu, M., D. L. Westphal, A. L. Walker, T. R. Holt, K. A. Richardson, and S. D. Miller. 2007. "COAMPS Real-Time Dust Storm Forecasting during Operation Iraqi Freedom." *Weather Forecasting* 22(1): 192–206. https://doi.org/10.1175/WAF971.1.

Liu, Z., et al. 2008. "Airborne Dust Distributions over the Tibetan Plateau and Surrounding Areas Derived from the First Year of CALIPSO Lidar Observations." *Atmospheric Chemistry and Physics* 8:5957–5977. https://doi.org/10.5194/acp-8-5045-2008.

Middleton, N., and A. S. Goudie. 2001. "Saharan Dust: Sources and Trajectories." *Transactions of the Institute of British Geographers* 26:165–181. https://doi.org/10.1111/1475-5661.00013.

Pospichal, B., D. B. Karam, S. Crewell, C. Flamant, A. Huenerbein, O. Bock, and F. Said. 2010. "Diurnal Cycle of the Intertropical Discontinuity over, West Africa Analyzed by Remote Sensing and Mesoscale Modelling." *Quarterly Journal of the Royal Meteorological Society* 136(1, SI): 92–106. doi:10.1002/qj.435.

Prospero, J., M., A. C. Delany, A. C. Delany, and T. N. Carlson. 2020. "The Discovery of African Dust Transport to the Western Hemisphere and the Saharan Air Layer: A History, *B." American Meteorological Society* 102:E1239–E1260, https://doi.org/10.1175/BAMS-D-19-0309.1.

Prospero, J., M., P. Ginoux, O. Torres, S. E. Nicholson, and T. E. Gill. 2002. "Environmental Characterization of Global Sources of Atmospheric Soil Dust Identified with the NIMBUS 7 Total Ozone Mapping Spectrometer (TOMS) Absorbing Aerosol Product." *Reviews of Geophysics* 40:1002. https://doi.org/10.1029/2000RG000095.

Pu, B., and Q. Jin. 2021. "A Record-Breaking Trans-Atlantic African Dust Plume Associated with Atmospheric Circulation Extremes in June 2020." *Bulletin of the American Meteorological Society*. https://doi.org/10.1175/BAMS-D-21-0014.1.

Rogowski, P., M. Otero, J. Hazard, T. Muschamp, S. Katz, and E. Terrill. 2021. "XMET—an Unattended Meteorological Sensing System for Austere Environments." *Journal of Atmospheric and Oceanic Technology* 38(1): 17–30. https://doi.org/10.1175/JTECH-D-20-0016.1.

Schweitzer, M. D., A. S. Salamo, et al. 2018. "Lung Health in Era of Climate Change and Dust Storms." *Environmental Research* 163:36–42. doi:10.1016/j.envres.2018.02.001.

Sinclair, S. N., and S. L. Jones. 2017. *Subjective-Mapping of Dust Emission Sources by Using MODIS Imagery: Reproducibility Assessment*. ERDC/TR-17-8. Vicksburg, MS: US Army Engineer Research and Development Center.

Washington, R., C. Bouet, G. Cautenet, E. Mackenzie, I. Ashpole, S. Engelstaedter, G. Lizcano, G. M. Henderson, K. Schepanski, and I. Tegen. 2009. "Dust as a Tipping Element: The Bodélé Depression, Chad." *Proceeds of the National Academy of Sciences of the United States of America* 106:20,564–20,571, Doi:10.1073/pnas.0711850106.

Washington, R., M. C. Todd, S. Engelstaedter, S. Mbainayel, and F. Mitchell. 2006. "Dust and the Low-Level Circulation over the Bodélé Depression, Chad: Observations from Bodex." *Journal of Geophysical Research* 111:D03201, doi:10.1029/2005JD006502.

Winker, D. M., W. H. Hunt, and M. J. McGill. 2007. "Initial Performance Assessment of CALIOP." *Geophys. Res. Lett*. 34:L19803.

Vaughan, A. Mark, Stuart A. Young, David M. Winker, Kathleen A. Powell, Ali H. Omar, Zhaoyan Liu, Yongxiang Hu, and Chris A. Hostetler. 2004. "Fully Automated Analysis of Space-Based Lidar Data: An Overview of the CALIPSO Retrieval Algorithms and Data Products. *Proc." SPIE* 5575, *Laser Radar Techniques for Atmospheric Sensing*. https://doi.org/10.1117/12.572024.

Appendix A: Technical Glossary of Meteorological Terms

This section provides the definitions set by the American Meteorological Society (AMS) for all terms identified with an asterisk throughout this report. For additional guidance on meteorological terminology, we recommend readers review information provided by the AMS Glossary of Meteorology website (http://glossary.ametsoc.org/wiki).

Aerosol, **Optical Depth (AOD)**—the optical depth due to extinction by the aerosol component of the atmosphere.

Aerosol optical depths typically decrease with increasing wavelength and are much smaller for longwave radiation than for shortwave radiation. Values vary widely depending on atmospheric conditions, but are typically in the range 0.02–0.2 for visible radiation.

Convection—In general, mass motions within a fluid resulting in transport and mixing of the properties of that fluid.

Convection, along with conduction and radiation, is a principal means of energy transfer. Distinction is made between free convection (gravitational or buoyant convection), motion caused only by density differences within the fluid; and forced convection, motion induced by mechanical forces such as deflection by a large-scale surface irregularity, turbulent flow caused by friction at the boundary of a fluid, or motion caused by any applied pressure gradient. Free and forced convection are not necessarily exclusive processes. On a windy day with overcast sky, the heat exchange between ground and air is an example of forced convection. On a sunny day with a little wind where the ground temperature rises, both kinds of convection take place.

Dewpoint—(or dewpoint temperature.) The temperature to which a given air parcel must be cooled at constant pressure and constant water vapor content in order for saturation to occur.

When this temperature is below 0°C, it is sometimes called the frost point. The dewpoint may alternatively be defined as the temperature at which the saturation vapor pressure of the parcel is equal to the actual vapor

pressure of the contained water vapor. Isobaric heating or cooling of an air parcel does not alter the value of that parcel's dewpoint, as long as no vapor is added or removed. Therefore, the dewpoint is a conservative property of air with respect to such processes. However, the dewpoint is nonconservative with respect to vertical adiabatic motions of air in the atmosphere. The dewpoint of ascending moist air decreases at a rate only about one-fifth as great as the dry-adiabatic lapse rate. The dewpoint can be measured directly by several kinds of dewpoint hygrometers or it can be deduced indirectly from psychrometers or devices that measure the water vapor density or mixing ratio.

Geopotential, **Height**—The height of a given point in the atmosphere in units proportional to the potential energy of unit mass (geopotential) at this height relative to sea level.

The relation, in SI units, between the geopotential height Z and the geometric height z is

$$Z = \frac{1}{g_0}\int_0^z g\,dz',$$

where g is the acceleration of gravity and g_0 is the globally averaged acceleration of gravity at sea level (g_0 = 9.80665 m s^{-2}), so that the two heights are numerically interchangeable for most meteorological purposes. Also, one geopotential meter is equal to 0.98 dynamic meter.

Haboob—An intense sandstorm or dust storm caused by strong winds, with sand and/or dust often lofted to heights as high as 1500 m (approximately 5000 ft), resulting in a *wall of dust* along the leading edge of the haboob that can be visually stunning. There is commonly a rapid and significant reduction in visibility and an increase in wind speed following the passage of the leading edge of a haboob, which can last for tens of minutes to a few hours. Haboobs are often caused by an atmospheric gravity or density current, such as thunderstorm outflow, but can also occur as a result of strong synoptic gradient winds, such as following a dryline or dry frontal passage. When a haboob is caused by a strong density current, the leading-edge wall of dust roughly conforms to the shape of the associated density current head. Haboobs occur fairly regularly in the arid and semiarid regions of the world and can occur in

any dry region. Sometimes they deposit enormous quantities of sand and/or dust.

The name comes from the Arabic word *habb*, meaning *to blow*. The term *haboob* originated as a description for wind and sandstorms/duststorms in central and northern Sudan, especially around the Khartoum area, where the average number is about 24 Per Year, with the Most Frequent Occurrences from May through September. However, the term is now commonly used to describe any wind-driven sandstorm or dust storm in arid or semiarid regions around the world, and haboobs have been observed in the Middle East/Arabian Peninsula, the Sahara Desert, central Australia, and the arid regions of southwest North America, from the Sonoran Desert of northwest Mexico and Arizona to the western portions of the Great Plains of the United States.

Intertropical, **Convergence Zone**—(also called *ITCZ*, equatorial convergence zone.) The axis, or a portion thereof, of the broad trade-wind current of the Tropics.

This axis is the dividing line between the southeast trades and the northeast trades (of the Southern and Northern Hemispheres, respectively). It is collocated with the ascending branch of the Hadley cell. At one time it was held that this was a convergence line along its entire extent. It is now recognized that actual convergence occurs only along portions of this line.

Jet, **Streak**—Relatively strong winds concentrated within a narrow stream in the atmosphere.

While this term may be applied to any such stream regardless of direction (including vertical), it is coming more and more to mean only a quasi-horizontal jet stream of maximum winds embedded in the midlatitude westerlies, and concentrated in the high troposphere. The question of the maintenance of the jet stream is a cardinal problem of theoretical meteorology. Two such jet streams are sometimes distinguished. The predominant one, the polar-front jet stream, is associated with the polar front of middle and upper-middle latitudes. Generally, it may be said to extend around the hemisphere, but like the polar front, it is discontinuous and varies greatly from day to day. A subtropical jet stream is found, at some longitudes, between 20° and 30° latitude and is strongest off the

Asian Coast. Currently, in the analysis of upper-level charts, a jet stream is indicated wherever it is reliably determined that the wind speed equals or exceeds 50 kn.

Mesoscale—Pertaining to atmospheric phenomena having horizontal scales ranging from a few to several hundred kilometers, including thunderstorms, squall lines, fronts, precipitation bands in tropical and extratropical cyclones, and topographically generated weather systems such as mountain waves and sea and land breezes.

From a dynamical perspective, this term pertains to processes with timescales ranging from the inverse of the Brunt–Väisälä frequency to a pendulum day, encompassing deep moist convection and the full spectrum of inertio-gravity waves but stopping short of synoptic-scale phenomena, which have Rossby numbers less than 1.

Mesoscale, **Convective System (Mcs)**—(abbreviated Mcs.) A cloud system that occurs in connection with an ensemble of thunderstorms and produces a contiguous precipitation area on the order of 100 km or more in horizontal scale in at least one direction.

An MCS exhibits deep, moist convective overturning contiguous with or embedded within a mesoscale vertical circulation that is at least partially driven by the convective overturning.

Mesoscale, **Convective Vortex**—A midlevel, warm-core low pressure center that develops within the stratiform region of a mesoscale convective system (MCS) as a result of latent heat release over a multihour time period. The cyclonic vortex has a diameter ranging from 50 to 200 km (31 to 124 mi) and a depth from 2.5 to 5 km (1.5 to 3.1 mi). An MCV can persist for 12 hr or more after its parent MCS has dissipated. A residual MCV may help initiate a subsequent episode of convection. An MCV that moves into tropical waters can serve as a nucleus for a tropical cyclone.

Ridge—(sometimes called *wedge*) In meteorology, an elongated area of relatively high atmospheric pressure, almost always associated with and most clearly identified as an area of maximum anticyclonic curvature of wind flow. The locus of this maximum curvature is called the ridge line. Sometimes, particularly in discussions of atmospheric waves embedded in the westerlies, a ridge line is considered to be a line drawn through all

points at which the anticyclonically curved isobars or contour lines are tangent to a latitude circle. The most common use of this term is to distinguish it from the closed circulation of a high (or anticyclone); but a ridge may include a high (and an upper-air ridge may be associated with a surface high) and a high may have one or more distinct ridges radiating from its center. The opposite of a ridge is a trough.

Synoptic-Scale—Used with respect to weather systems ranging in size from several hundred kilometers to several thousand kilometers; the scale of migratory high- and low-pressure systems (frontal cyclones) of the lower troposphere.

Trough—In meteorology, an elongated area of relatively low atmospheric pressure; the opposite of a ridge. The axis of a trough is the trough line. This term is commonly used to distinguish the previous condition from the closed circulation of a low (or cyclone), but a large-scale trough may include one or more lows, an upper-air trough may be associated with a lower-level low, and a low may have one or more distinct troughs radiating from it.

Upper, **Air Sounding**—A measurement of atmospheric conditions aloft, above the effective range of a surface weather observation.

This is a general term but is usually applied to those observations that are used in the analysis of upper-air charts (as opposed to measurements of upper-atmospheric quantities primarily for research). Among the elements evaluated are pressure, temperature, relative humidity (e.g., by radiosonde aircraft observations), and wind speed and direction (e.g., by rawinsonde, aircraft, or wind profiling radars). Also, some mountain stations are high enough and exposed enough so that their observations may be included in the upper-air network at their elevation.

See also meteorological rocket, radiosonde balloon.

Wave, **Train**—A superposition of waves propagating in the same direction and with almost equal phase speeds.

Abbreviations

AEJ	Africa Easterly Jet
AERONET	Aerosol Robotic Network
AMS	American Meteorological Society
AOD	Aerosol optical depth
CALIPSO	Cloud-Aerosol lidar and Infrared Pathfinder Satellite Observation
DT/DB	Dark-Target/Deep Blue
ECMWF	European Centre for Medium-Range Weather Forecasts
ITCZ	Intertropical Convergence Zone
MCS	Mesoscale convective system
MODIS	Moderate Resolution Imaging Spectroradiometer
MSG	Meteosat Second Generation
SEVIRI	Spinning Enhanced Visible InfraRed Imager
U	West-east; zonal
UK Met Office	United Kingdom Meteorology Office
V	South-north; meridional

REPORT DOCUMENTATION PAGE

Form Approved

OMB No. 0704-0188

1. REPORT DATE (DD-MM-YYYY)	2. REPORT TYPE	3. DATES COVERED (From–To)
February 2023	Final Report	FY21

4. TITLE AND SUBTITLE

Establishing a Series of Dust Event Case Studies for North Africa

5a. CONTRACT NUMBER

5b. GRANT NUMBER

5c. PROGRAM ELEMENT

6. AUTHOR(S)

Kent H. Sparrow and Sandra L. LeGrand

5d. PROJECT NUMBER

5e. TASK NUMBER

5f. WORK UNIT NUMBER

7. PERFORMING ORGANIZATION NAME(S) AND ADDRESS(ES)

US Army Engineer Research and Development Center (ERDC)
Coastal and Hydraulics Laboratory (CHL)
3909 Halls Ferry Road
Vicksburg, MS 39180-6199

Geospatial Research Laboratory
7701 Telegraph Road
Alexandria, VA 22315

8. PERFORMING ORGANIZATION REPORT NUMBER

ERDC SR-23-1

9. SPONSORING / MONITORING AGENCY NAME(S) AND ADDRESS(ES)

Air Force Lifecycle Management Center and
United Kingdom Meteorology Office
Hanscom AFB, MA 01731-2103

10. SPONSOR/MONITOR'S ACRONYM(S)

AFLCMC

11. SPONSOR/MONITOR'S REPORT NUMBER(S)

12. DISTRIBUTION / AVAILABILITY STATEMENT

Approved for public release; distribution is unlimited.

13. SUPPLEMENTARY NOTES

Air Force Lifecycle Management Center; MIPR F2BDAN1239G003

14. ABSTRACT

Dust aerosols often create hazardous air quality conditions that affect human health, visibility, agriculture, and communication in various parts of the world. While substantial progress has been made in dust-event simulation and hazard mitigation over the last several decades, accurately forecasting the spatial and temporal variability of dust emissions continues to be a challenge. This report documents an analysis of atmospheric conditions for a series of dust events in North Africa. The researchers highlight four analyzed events that occurred between January 2016 to present in the following locations: (1) the western Sahara Desert; (2) East Algeria and the Iberian Peninsula; (3) Chad-Bodélé Depression; (4) Algeria and Morocco. For each event, the researchers developed an overview of the general synoptic, mesoscale, and local environmental forcing conditions that controlled the event evolution and used a combination of available lidar data, surface weather observations, upper-air soundings, aerosol optical depth, and satellite imagery to characterize the dust conditions. These assessments will support downstream forecast model evaluation and sensitivity testing; however, the researchers also encourage broader use of these assessments as reference case studies for dust transport, air quality modeling, remote sensing, soil erosion, and land management research applications.

15. SUBJECT TERMS

Africa, North, Air quality, Dust, Dust storms, Geospatial data

16. SECURITY CLASSIFICATION OF:			17. LIMITATION OF ABSTRACT	18. NUMBER OF PAGES	19a. NAME OF RESPONSIBLE PERSON
					Kent H. Sparrow
a. REPORT	b. ABSTRACT	c. THIS PAGE			19b. TELEPHONE NUMBER (include area code)
Unclassified	Unclassified	Unclassified	SAR	69	601.480.2309